Nanoscale Horizons

ROYAL SOCIETY OF CHEMISTRY

REVIEW

View Article Online
View Journal | View Issue

Check for updates

Cite this: *Nanoscale Horiz.*, 2021, 6, 676

Luminescent copper indium sulfide (CIS) quantum dots for bioimaging applications

Giacomo Morselli, *[a] Marco Villa,[a] Andrea Fermi,[a] Kevin Critchley[b] and Paola Ceroni *[a]

Received 10th May 2021,
Accepted 9th July 2021

DOI: 10.1039/d1nh00260k

rsc.li/nanoscale-horizons

Copper indium sulfide (CIS) quantum dots are ideal for bioimaging applications, by being characterized by high molar absorption coefficients throughout the entire visible spectrum, high photoluminescence quantum yield, high tolerance to the presence of lattice defects, emission tunability from the red to the near-infrared spectral region by changing their dimensions and composition, and long lifetimes (hundreds of nanoseconds) enabling time-gated detection to increase signal-to-noise ratio. The present review collects: (i) the most common procedures used to synthesize stable CIS QDs and the possible strategies to enhance their colloidal stability in aqueous environment, a property needed for bioimaging applications; (ii) their photophysical properties and parameters that affect the energy and brightness of their photoluminescence; (iii) toxicity and bioimaging applications of CIS QDs, including tumor targeting, time-gated detection and multimodal imaging, as well as theranostics. Future perspectives are analyzed in view of advantages and potential limitations of CIS QDs compared to most traditional QDs.

Published on 15 2021. Downloaded on 03.10.2024 13:38:38.

1. Introduction

In the last few decades, nanomaterials and especially nanoparticles have emerged as interesting probes for biomedical purposes,[1] *e.g.* as contrast agents for diagnostic applications, including magnetic resonance imaging (MRI),[2,3] computed tomography (CT),[4] positron emission tomography (PET) and single photon emission computed tomography (SPECT),[5] *et cetera*.[6] In particular, semiconducting nanocrystals, also called quantum dots (QDs), are effective tools for optical imaging.[7–9] QDs show undoubted advantages over conventional molecular probes, which render them ideal luminophores: they possess size and shape-dependent optical properties, and therefore the absorption and the emission features can be modulated and

[a] *Department of Chemistry "Giacomo Ciamician", University of Bologna, Bologna, 40126, Italy. E-mail: giacomo.morselli2@unibo.it, paola.ceroni@unibo.it*
[b] *School of Physics and Astronomy, University of Leeds, Leeds, LS2 9JT, UK*

Giacomo Morselli

Giacomo Morselli received his Master's degree in Photochemistry and Molecular Materials from the University of Bologna in 2018. The same year, he joined the group of professor Paola Ceroni as PhD student in "Nanoscience for Medicine and the Environment". During his PhD studies, he was hosted in Dr Kevin Critchley group, where he learnt how to synthesize copper indium sulfide quantum dots. His research is focused on the synthesis and characterization of semiconducting nanoparticles.

Marco Villa

Marco Villa completed his Master's degree in Photochemistry and Molecular Materials at the University of Bologna, Italy, under the supervision of Prof. Ceroni. He moved to France at Aix-Marseille Université, under the supervision of Prof. Gingras for a doctoral position in a joint agreement with the University of Bologna under the co-supervision of Prof. Ceroni. After obtaining his doctoral degree, he returned to Italy at the university of Bologna to work with Prof. Ceroni with a post-doctoral fellowship. In the last years, his research was focused on the synthesis and characterization of semiconducting nanomaterials and persulfurated aromatic compounds.

This journal is © The Royal Society of Chemistry 2021

Published on 15 2021. Downloaded on 03.10.2024 13:38:38.

controlled during the synthetic process;[10,11] their high photostability allows them to resist to long-time or multiple irradiations without bleaching;[12] most importantly, the possibility to engineer them may achieve new properties and functions.[13,14] For instance, the functionalization with binders for specific biomarkers can permit to accomplish an active targeting, guiding the nanoparticle towards a precise target site;[15] the coupling with different responsive systems can enable multi-modal imaging (*i.e.* the combination between different diagnostic imaging techniques)[13,16] or even theranostics (*i.e.* integrating the diagnostic tool provided by the QD with a therapeutic one enabled by the functionalizing moiety).[17]

QDs materials that have been extensively studied for many applications, including interconversion between light and electric energy,[18–20] photocatalysis[21] and sensing,[22] are made of group II–VI or IV–VI elements. Unfortunately, such systems contain toxic heavy metals, namely cadmium and lead, which hinder their utilization in biological systems.[13,23] Many efforts have been addressed to decrease the harmfulness of those systems by encapsulating the core of the emitting nanoparticle in a shell of a more inert semiconductor (typically ZnS or ZnSe)[24] or a polymeric layer,[25] to avoid the leakage of toxic cations into the biological system. However, the resultant increased dimensions can be detrimental for the elimination of the nanoparticle from the body. In fact, renal excretion, which is the preferential way of clearance, is exclusive for nanoparticles with smaller hydrodynamic diameters (*ca.* 5 nm), due to the limited filtration-size threshold in kidneys.[26]

Those issues compelled nanomedicine researchers to investigate new systems which could display a better biocompatibility maintaining the advantages of a stable, bright and tunable emission. Therefore, cadmium and lead-free QDs, such as silver-based QDs,[27] silicon[28–30] and germanium[31,32] nanoparticles have been explored.[9] One of the most promising alternatives has been offered by copper indium disulfide ($CuInS_2$, CIS) QDs.

Copper indium sulfide is a ternary I–III–VI_2 type semiconductor (I = Cu^+, III = In^{3+}; VI = S^{2-}) usually found in nature as a mineral called ''roquesite'',[33] characterized by a bulk direct band gap of approximately 1.5 eV.[34] When the dimensions of the material are reduced to a few nanometers, quantum confinement effects arise, and the properties of the semiconductor, such as the bandgap, become size dependent.[35] It is interesting to note how the main advantages of CIS QDs rely not only in a diminished toxicity (compared to conventional QDs), but also their peculiar optical properties which are considered highly suitable for bioimaging applications.[36] As a matter of fact, they are characterized by (i) high molar absorption coefficients that cover the entire visible spectrum (*ca.* 10^4–10^5 M^{-1} cm^{-1});[37] (ii) the photoluminescence quantum yield (PLQY), which can reach elevated values (up to 70%);[38] (iii) unlike conventional QDs, defects in the crystal lattice are well tolerated; (iv) the emission can be tuned not only by varying the size of the nanoparticle,

Andrea Fermi

Andrea Fermi obtained his PhD in Chemistry in 2013 from the University of Bologna and Aix-Marseille Université, under the supervision of Prof. Paola Ceroni and Prof. Marc Gingras. After postdoctoral stays at the University of Namur, Cardiff University and University of Bologna, he is now junior researcher at the Department of Chemistry at the University of Bologna. His research mainly focuses on photoinduced processes in supramolecular assemblies and nanomaterials, and on opto-electronic properties of molecular materials.

Kevin Critchley

Kevin Critchley studied Physics and Electronics with Instrumentation at the University of Leeds, United Kingdom, where he also earned his PhD, in 2005, under the supervision of Prof. S. D. Evans. He continued at Leeds as a postdoctoral researcher until 2007, when he joined Prof NA Kotov's group at the University of Michigan as an EU Marie Curie Fellow. In 2009, he returned to the University of Leeds and by 2010 had began to build his own research group. In 2019 he was promoted an Associate Professor in the School of Physics and Astronomy. His research interests include colloidal quantum dots, quantum rods, nanowires, gold nanomaterials, and surface functionalisation.

Paola Ceroni

Paola Ceroni is full professor at the University of Bologna. In 1998 she obtained her PhD degree in Chemical Sciences at the University of Bologna, after a period in the United States (Prof. Allen J. Bard's Laboratory). Current research is focused on photoactive supramolecular systems and nanocrystals for energy conversion and imaging. Her research on luminescent silicon nanocrystals was funded by an ERC Starting Grant PhotoSi and an ERC Proof of Concept SiNBiosys.

Published on 15 2021. Downloaded on 03.10.2024 13:38:38.

but also the composition, and this is important if specific dimensions need to be preserved; (v) most importantly for biomedical applications, the emission of CIS QDs spans the red to near-infrared (NIR) spectral range, therefore the so-called biological transparency window, the wavelengths that most penetrate biological tissues; (vi) their photoluminescence is characterized by long lifetimes (hundreds of nanoseconds). The latter is important to enable bioimaging techniques with increased signal-to-noise ratio.[35,36,39–42]

This review will cover the general procedures used to synthesize stable CIS QDs and the typical methods to enhance their colloidal stability in aqueous environment (Section 2), which is an indispensable requisite for bioimaging applications. Section 3 will focus on the photophysical properties of CIS QDs and the studies related to the control and manipulation of the photoluminescence. Sections 4 and 5 will be dedicated to the bioimaging applications of CIS QDs, ranging from the first developments to the most recent studies and eventually the future perspectives that these promising QDs are reserving. Other applications, including solar energy conversion, luminescent solar concentrators, sensing and biosensing, photocatalysis and light-emitting diodes will not be discussed and the readers will be addressed to other reviews.[35,36,43,44]

2. Synthesis

General procedures

The synthesis of the nanoparticle represents an important process not only for CIS, but for every QD. In general, this step defines the composition, the size and shape of the QD, of which the photophysical properties are dependent.

During the synthesis, the crystallographic structure of the nanoparticle is also determined. Because it is paramount for the luminescent properties, the crystallography of CIS will be briefly discussed. Bulk $CuInS_2$, at room temperature, crystallizes only in the tetragonal structure of chalcopyrite (CP, $CuFeS_2$), in which the cations occupy ordered positions. At higher temperatures, a random distribution of In^{3+} and Cu^+ is more likely to occur and the stoichiometry of the compound becomes more flexible. Therefore, at 980 °C, CIS can achieve a zinc blende (ZB)-like structure, which is similar to CP one, but with a random swap of the cations, and at 1045 °C, an hexagonal wurtzite (WZ)-like structure.[45] The crystallographic structures are reported in Fig. 1.

At the nanoscale, CIS can crystallize in each structure at the same temperature, depending on the adopted synthetical methodology.[46] CP structure (Fig. 1a) exhibits a cation ordering in which each sulfide ion is surrounded by two In^{3+} and two Cu^+ ions. The Cu–S and In–S bond lengths are quite different, and this causes a tetragonal distortion of the crystal lattice. This results in a low band gap energy, an abundance of intrinsic defects and a broader emission compared to cadmium-based QDs.[39,40,47] As stated before, ZB structure (Fig. 1b) is comparable to CP and it is also difficult to distinguish due to their similar XRD and electron diffraction patterns. For CP and ZB structures, the displacement of the cations can lead to a non-stoichiometric

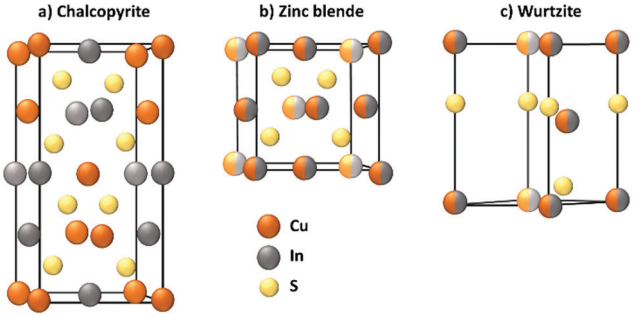

Fig. 1 Crystallographic structures of (a) chalcopyrite, (b) zinc blende and (c) wurtzite CIS.

CIS compound which could be useful for photovoltaic applications because of the formation of n-type and p-type nanocrystals.[48] WZ structure (Fig. 1c) is characterized by a superior order in which an anionic lattice is interlaced with domains of ordered cations sublattices.[49] The mechanism of its formation is more defined with respect to CP CIS QDs: it is well-known that CIS QDs with a WZ-like structure will grow if a Cu_2S intermediate is formed first.[50,51] However, their emissive properties are reported to be usually worse than both CP and ZB CIS QDs, and therefore this requires attention during the synthetic process, if the scope is to obtain highly emitting nanoparticles.[39]

A well-controlled synthesis of CIS QDs is generally considered to be challenging because of the different affinity of the cations with respect to the anion. According to the HSAB (hard/soft acid/base) theory, Cu^+ and In^{3+} are, respectively, a soft and a hard Lewis acid, while S^{2-} is a soft Lewis base. Consequently, if the reaction conditions are not adjusted, precipitation of Cu_2S can occur instead of the formation of the QDs, or CIS with an undesired WZ-like structure can grow. To balance the reactivity of the reactants, three main strategies have been developed. The reactivity of copper and indium cations can be simultaneously adjusted by including different types of ligands in the reaction mixture, for instance thiols (*i.e.* soft Lewis bases, therefore stabilizing Cu^+) together with carboxylates (hard Lewis bases, to control the reactivity of In^{3+}).[52,53] As an alternative, an excess of thiol can be introduced, to accomplish the triple function of sulfur source, solvent and copper stabilizer.[38] Another option is provided by the use of a precursor containing both the cations, namely $(PPh_3)_2CuIn(SCH_3CH_2)_4$:[54,55] in the reaction mixture, its decomposition releases the same quantities of copper and indium, therefore avoiding the formation of binary compounds.

While there are many synthetic approaches to obtain CIS QDs with controllable sizes, shapes and crystallographic structures by varying the kinds of precursors, solvents, ligands and reaction conditions,[35] their complete description is beyond the scope of this review.

The synthetic processes can be divided into three main categories: hot-injection techniques, heating-up (or non-injection) methods, and templated-assisted approaches.

Hot-injection techniques rely on the strict control and separation of nucleation and growth phases: in order to form a monodisperse sample, the nanocrystals should nucleate at

 This journal is © The Royal Society of Chemistry 2021

Published on 15 2021. Downloaded on 03.10.2024 13:38:38.

the same time and grow with the same rate. A solution of the cationic precursors is heated up to high temperatures, in the presence of a high-boiling solvent and the ligand molecule. Then, a room-temperature solution of the anion precursor is rapidly injected into the reaction mixture. The high temperature of the solution of the first component leads to a rapid single nucleation, which is immediately quenched by the lowering of the temperature due to the injected solution of the second component. Therefore, a low process of growth begins. The reaction will be quenched at room temperature, and the isolation and purification of the QDs can be performed (Fig. 2a).[53]

Conversely, heating-up techniques consist in a one-pot procedure in which the cationic precursors (*e.g.*, copper(I) iodide and indium(III) acetate) are mixed together with an excess of thiol (typically 1-dodecanethiol) and a non-coordinating solvent (such as octadecene, ODE). At high temperatures (*ca.* 180 °C), the alkanethiol molecules decompose and release sulfur ions, which provides the anions for the CIS crystal growth. Enhancing the temperature (over 200 °C), the color of the suspension varies from yellow to dark red, indicating the nucleation and subsequent growth of the QDs. When the desired sizes are reached, the reaction is quenched by decreasing the temperature with a cold-water bath.[38]

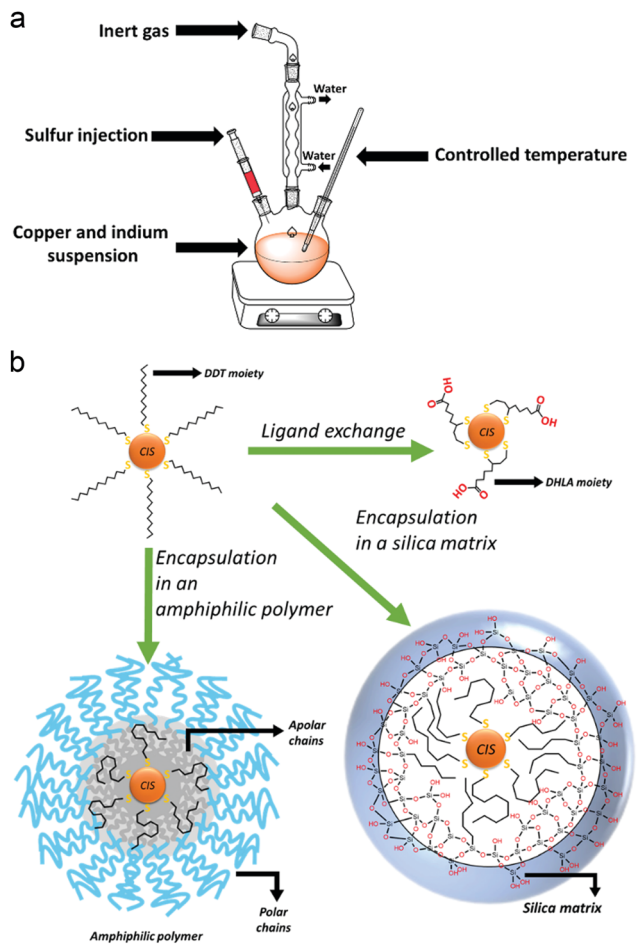

Fig. 2 (a) Schematic representation of an organic phase synthesis of CIS QDs. (b) Schematization of the three main methods to obtain water-suspendable CIS QDs from QDs synthesized in organic medium. Here, DDT = 1-dodecanethiol, DHLA = dihydrolipoic acid.

While the best size and shape controls can be achieved by hot-injection and heating-up procedures, a template can be useful to select the crystallographic structure of the resulting CIS QDs. Here, the formation of a binary compound which shares the crystallographic structure of the desired compound is firstly synthesized (*e.g.* tetragonal indium sulfides as templates for CP CIS QDs[56] or hexagonal copper sulfides for WZ CIS QDs[51,57]); then, a partial cation exchange follows, to achieve the ternary copper indium sulfide compound.

To render the nanoparticles more suitable for bioimaging applications as photoluminescent probes, it can be useful to enhance or modify the optical properties by alloying or embedding the nanoparticle in a shell of an appropriate semiconductor (see Section 3 for further details). Doping the QD with additional cations (as zinc,[58] silver,[59] gallium,[60] tin,[61] gadolinium,[62] *et cetera*), thus forming alloyed systems, is made possible due to the high tolerance of CIS QDs towards lattice defects and their non-stoichiometry. Usually, in the syntheses, the precursor of the extra cation is added in the reaction mixture together with copper and indium before the crystallization occurs, but it is also possible to perform a partial cation exchange on already formed CIS QDs.[63] The emissive properties of CIS QDs, as well as their chemical stability, drastically enhance by covering the nanoparticles with a shell of a suitable semiconductor. Zinc(II) sulfide is a stable, non-toxic, semiconductor with a wide bandgap (3.5 eV), that shows a low lattice mismatch (*ca.* 2%) with copper indium sulfide, which permits an epitaxial growth. Zinc(II) sulfide, thanks to these properties, is one of the best choices to obtain a type-I core–shell system.[38] Despite several procedures being developed,[35] the zinc precursor is usually added to the preformed CIS QD synthesis solution and the temperature raised to 210 °C to initiate the shell formation. The temperature is typically maintained for 0.5 to 2 h. Nonetheless, it has been noticed that this reaction is also accompanied by other processes, such as the diffusion of Zn(II) into the lattice, or a partial cation exchange, which can further modify the optical properties, including a blue-shift of the emission peak.[43]

Phase transfer into water and bio-conjugation

Major emphasis will be given to the methods used to render CIS QDs colloidally stable in aqueous solutions, which is essential for bioimaging applications. The methods examined so far are performed in organic media, and the resulting nanoparticles are usually stabilized by an organic hydrophobic shell. Several approaches allow to synthesize directly CIS QDs in aqueous phase.[64–67] In this case, the syntheses are carried out in presence of water-soluble thiol derivatives, such as thioglycolic acid, mercaptopropionic acid, thiol-derivatized poly(ethylene) glycol or glutathione. For instance, it is possible to synthesize the CIS core by mixing $CuCl_2$ and $InCl_3$ in the presence of an aqueous solution of sodium citrate and L-glutathione. Then, sodium sulfide is injected as sulfur source, while zinc acetate and thiourea are used to make the shell grow.[64] Another interesting approach consists in the synthesis of biocompatible water-suspendable CIS QDs *via* a biomineralization process

Published on 15 2021. Downloaded on 03.10.2024 13:38:38.

that occurs in presence of an enzyme.[68] Microwave-assisted methods have also been introduced to improve the synthesis.[69] The nanoparticles are synthesized in basic water, in the presence of copper(II) nitrate, indium(III) chloride, sodium sulfide and glutathione. Irradiation in a microwave vessel leads to the formation of the CIS core. Also, the shell can be obtained by irradiation, after the addition of further sodium sulfide and zinc acetate. Recently, it has been reported an aqueous synthesis of CIS/ZnX (X = S, Se) stabilized with glutathione where the anions were electrochemically generated.[70] Despite the low cost and toxicity of those methods, the so-obtained nanoparticles are reported not to possess high quality properties;[43] therefore, it is common to perform the synthesis of CIS QDs in organic phase and then transfer the nanoparticles in water.

Phase transfer could be accomplished by three main methodologies of surface modification: ligand exchange, encapsulation in amphiphilic molecules or in a silica shell.

Ligand exchange consists in replacing the original ligands stabilizing the nanoparticles in organic phase with hydrophilic organic ligands. When thiols are used as ligands during the synthesis, their replacement can occur if the substituting molecule possesses a superior number of anchoring groups. For instance, dodecanethiol can be exchanged with dihydrolipoic acid (DHLA, 2 thiol moieties).[71] As an alternative it is possible to introduce long chain amines (such as oleylamine)[72,73] or phosphines[51] in a mixture with the thiols as stabilizers during the synthesis of the nanoparticles. The bonding between those molecules and the surface of the QD is more labile than the one with thiols. This allows to efficiently substitute them with other water-solubilizing thiols (*i.e.* mercaptopropionic acid) at a lower temperature. Unfortunately, ligand exchange is reported to lower the PLQY due to the reduction of the ZnS shell and consequent increase in surface trap states.

A different option consists in maintaining the apolar ligands utilized during the synthesis in the organic phase and encapsulating the nanoparticle in an amphiphilic polymer or micelles.[74–76] The hydrophobic groups present on the molecule interact in a non-covalent way with the apolar ligands of the QD, while the polar moieties allow a good dispersibility in water. For instance, it is reported[74] the coating of DDT capped CIS/ZnS core–shell QDs with an amphipol poly(maleic anhydride-*alt*-1-tetradecene), 3-(dimethylamino)-1-propylamine derivative, yielding water-suspendable systems stable at various pH. On the other hand, by silanization, it is possible to realize biocompatible water-suspendable silica-embedded CIS/ZnS QDs.[77,78] The three main mechanisms to accomplish phase transfer into water are represented in Fig. 2b.

Concerning *in vivo* applications, functionalization with poly(ethylene)glycol (PEG) or coating with a zwitterionic surface is important due to the limited opsonization of the nanoparticle and the enhanced circulation time. Briefly, it is well-known that when nanoparticles are administered, a variety of serum proteins (immunoglobulins, albumin, *et cetera*) bind to their surface. Those proteins are recognized by receptors overexposed on macrophage cell surfaces, which engulf the nanoparticle (*i.e.* phagocytosis) and remove them from circulation, driving them to reticuloendothelial system (RES) organs (*e.g.*, liver and spleen) to be degraded and excreted. The serum proteins which bind to the nanoparticles are also named "opsonins", and the process of adsorption is called "opsonization". PEG and zwitterionic groups overexpressed on the nanoparticles show to diminish the nonspecific interactions between the nanoparticle and the serum proteins, reducing opsonization.[79–81] Permadi *et al.*[82] introduced a PEG moiety *via* non-covalent interaction with the organic ligands. Encapsulation in a human serum albumin functionalized with PEG was performed by Kim *et al.*[83] In another study,[84] PEG with an average molecular weight of 400 Da was used as a non-coordinating solvent for direct synthesis of biocompatible ZnCuInS/ZnS nanoparticles in water. Direct PEGylation can be performed using a thiol derivatized poly(ethylene)glycol during the synthetic process.[66] Ligand exchange between original TOP ligands with PEG-SH,[85] or the ester of dihydrolipoic acid and poly(ethylene glycol)[86] are also reported.

If the modification of the surface of CIS QDs introduces molecules comprising a new, free reactive moiety (*e.g.*, carboxylic acids, amines, or alkynes) a further functionalization can occur. If this "post-functionalization" tethers a biomolecule (such as a protein, aptamers, amino acids, nucleic acids, *et cetera*) to the QD, the reaction is called bio-conjugation. Bio-conjugations are fundamental for several bioimaging techniques related to active targeting, as several biomolecules (*e.g.* folic acid,[87] tripeptides Lys-Pro-Val,[88] *et cetera*, *vide infra*) are recognized by specific receptors.

The usual bio-conjugation techniques are here reported. If carboxylic acids are overexpressed, an amide coupling can take place in the presence of an amine (and *vice versa*) and suitable coupling reagents. Namely carbodiimides such as 1-ethyl-3-(3-dimethylaminopropyl) carbodiimide hydrochloride (EDC), which converts the carboxylic moiety in an activated *O*-acylisourea, are widely used accompanied by *N*-hydroxy-succinimides (NHS or its sulfo-derivative) which transforms the *O*-acylisourea in an activated ester selectively reactive towards amines.[75,89] Other bio-conjugation techniques are reported for various QDs, including SMCC-mediated coupling between amines and thiols, azide–alkyne click-chemistry, hydrazone ligations and non-covalent bio-conjugation. Non-covalent bio-conjugation, in particular, can be performed through electrostatic interactions, encapsulation or interaction between complementary molecules (*e.g.* streptavidin–biotin).[90]

3. Photophysical properties

Bulk CIS is a semiconductor, and its direct band gap is approximately 1.5 eV. Therefore, visible light can be absorbed by the bulk material. Absorption results in the promotion of an electron from the valence to the conduction band of the semiconductor. This generates a couple of charge carriers, *i.e.* an exciton, constituted by an electron (e^-) in the conduction band and a positive hole (h^+) in the valence band. The medium distance between the charge carriers is called the exciton Bohr

 This journal is © The Royal Society of Chemistry 2021

Published on 15 2021. Downloaded on 03.10.2024 13:38:38.

radius, which, in the case of CIS, is about 4.1 nm. In colloidal dispersions of a semiconducting material, when the particle diameter is smaller than ~8 nm, the exciton is confined to the physical borders of the nanoparticle and, therefore, quantum confinement effects arise. As a result, the photophysical properties of semiconducting nanocrystals are strictly related to the size of the particles; consequently, larger band gaps are observed for smaller nanoparticles. To support this, some researchers[91] provided a comprehensive theoretical analysis on the relationship between size of the CIS QDs and their energy gap. Accordingly, the absorption spectrum can be varied over the entire visible range (Fig. 3a).[53] Booth *et al.*[37] provided an empirical derived formula to compute the molar absorption coefficient depending on the size of the nanoparticles at 3.1 eV and at the lowest energy electronic transition, showing high values (*ca.* 10^4–10^5 M^{-1} cm^{-1}). As compared to other popular binary semiconducting nanocrystals (*e.g.*: CdS, CdSe, ZnS, *etc.*), the absorption spectra of CIS QDs generally do not display well-defined exciton bands, while a broad shoulder with a long tail joining the NIR region is usually observed.[92] This is likely due to a combination of factors such as the inherent electronic properties of the ternary semiconductor, irregularity in the composition and distribution of the sample and size/shape inhomogeneities.[53] Most importantly, due to their direct band gap, the molar absorption coefficient of CIS QDs is usually much larger compared to those of other biocompatible QDs with promising bioimaging applications, such as silicon nanocrystals (*e.g.*: for 3 nm WZ CIS QDs, $\varepsilon_{400\,nm} = 3 \times 10^5$ M^{-1} cm^{-1};[93] 3 nm silicon nanocrystals: $\varepsilon_{400\,nm} = 3 \times 10^4$ M^{-1} cm^{-1}).[29,94] In addition to electronic transition bands in the visible spectrum, CIS quantum dots can display broad localized surface plasmon resonance bands in the NIR range, that might be due to the presence of point defects, namely copper vacancies.[95,96]

Following the excitation, a radiative deactivation of the exciton, *i.e.*, photoluminescence, can take place. Despite there is no universal agreement on the mechanism of the photoluminescence in CIS QDs, it is well-accepted that it is not associated to a band edge transition, but originates from defects of the crystal structure, including vacancies and antisites. Among the various hypotheses, the most accepted ones are the recombination of a donor–acceptor pair (DAP) and a free-to-bound recombination.[35,36,38–40,55,97] It has been proposed that the two mechanisms coexist, but only one is relevant depending on the stoichiometry of the nanoparticle (DAP recombination is dominant for indium-rich CIS QDs).[36]

The size-dependent emission of CIS QDs can be varied within the spectral region spanning the red to near-infrared range (Fig. 3).[98] This is an interesting feature for bioimaging applications, because it overlaps with the biological transparency window, as shown in Fig. 4.

The emissive properties of CIS QDs show important differences with other direct band gap semiconductor nanoparticles.[40] From the emission dynamics perspective, while prototypical CdSe QDs show a lifetime of 10–30 ns at room temperature, emission decays are generally longer for ternary semiconducting nanocrystals: non-shelled CIS QDs usually display a biexponential decay,[38] with a shorter component in the range of 10^0–10^1 ns and a longer one in the order of 10^2 ns. Due to size inhomogeneities and the overlapping of various vibro-electronic transitions,[55] CIS QD emission bands are characterized by a higher FWHM (about 100 nm) when compared to conventional QDs. Further studies recently demonstrated that the preferential localization of the excitonic hole on Cu sites plays an essential role on the broadening of the photoluminescence signals.[99,100] Another considerable dissimilarity consists in usually high Stokes shifts (200–300 meV), caused by the presence of different electronic states involved in absorption and emission, which diminishes the probability of reabsorption.[101] Interestingly, the optical properties can be tuned not only by varying the nanoparticle size, but also modifying the composition and the metal-to-metal stoichiometry of the compound.[39] A blue-shift of

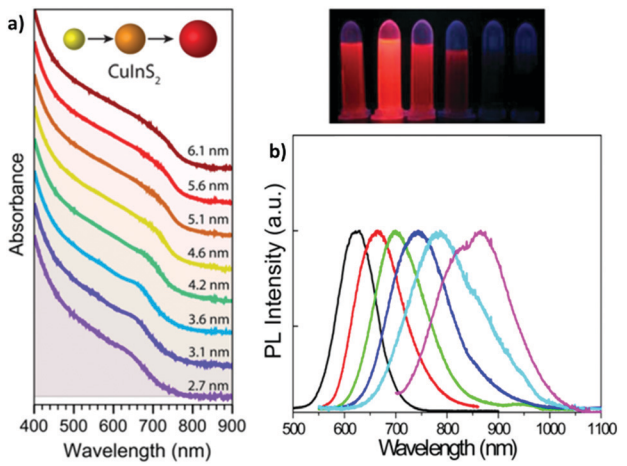

Fig. 3 (a) Absorption spectra (plus offset) of WZ CIS QDs ranging from 2.7 to 6.1 nm in size. Adapted from ref. 93. Copyright (2015) American Chemical Society. DOI: 10.1021/acsnano.8b03641. (b) Emission spectra (and digital photographs under UV light) of CIS QDs with different size. Reprinted (adapted) with permission from ref. 98. Copyright (2012) American Chemical Society.

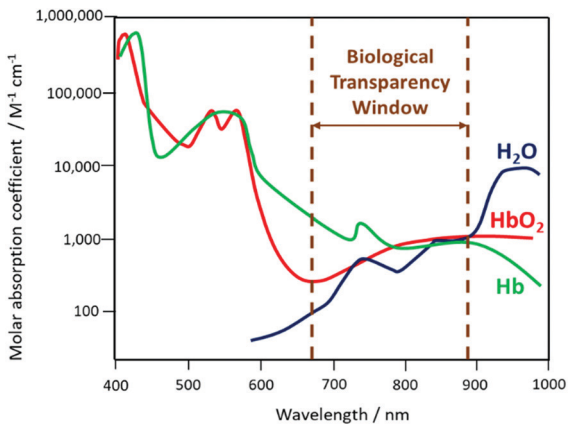

Fig. 4 Schematization of the biological transparency window within the absorption spectra (logarithmic scale) of haemoglobin (Hb), oxygenated haemoglobin (HbO_2) and water.

Published on 15 2021. Downloaded on 03.10.2024 13:38:38.

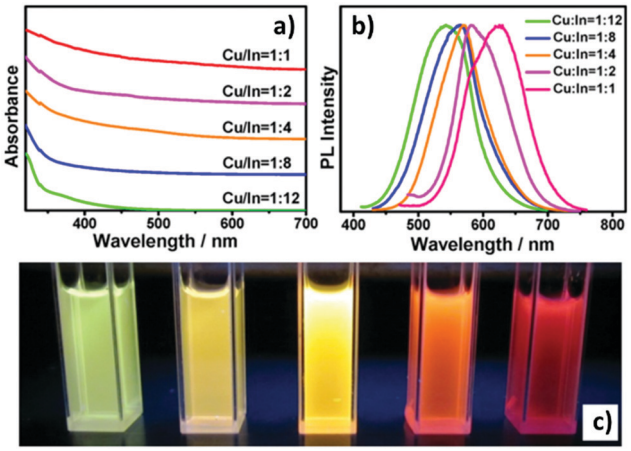

Fig. 5 UV-vis absorption (a) and PL (b) spectra of Cu–In–S/ZnS core/shell QDs with different Cu/In ratios in the cores; digital photograph (c) of Cu–In–S/ZnS core/shell QDs under UV-light irradiation. The QDs with different PL colors were all capped by two monolayers of the ZnS shell. Reprinted with permission from ref. 64. Copyright (2013) American Chemical Society.

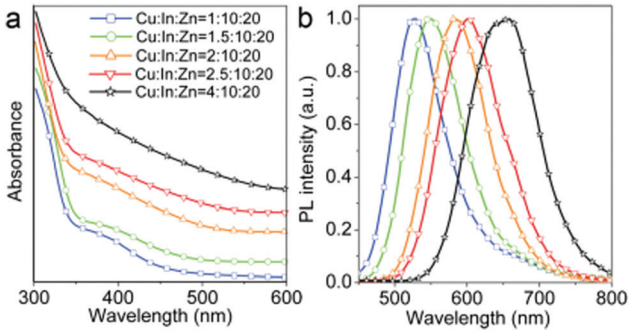

Fig. 6 (a) Absorption and (b) emission spectra of Zn-alloyed CIS QDs with different cation precursors ratio (λ_{ex} = 425 nm). Reproduced from ref. 105 with permission from The Royal Society of Chemistry.

both absorption and emission spectra occurs when decreasing the ratio [Cu]/[In] (Fig. 5).[64] Also, an increase of the band gap was reported. This was attributed to the strong contribution of Cu 3d-orbital to the valence band: a Cu deficiency results in a lowering of the occupied levels,[102] while an enhancement of PLQY is observed (up to 30%).[40] The dependence between PLQYs and [Cu]/[In] ratios relies on donor–acceptor pair luminescence mechanisms and the introduction of defects responsible of radiative decays.[48]

The PLQY drastically increases when CIS QDs is shelled with a higher band gap semiconductor (*i.e.*, a type I core–shell QDs). For CP CIS QDs, PLQY is reported to enhance from 5–10% to *ca.* 70% with a ZnS shell,[38] and usually the short-lived emitting component is not detected. These aspects are connected with the suppression of surface states that act as trap for the charge carriers, either reducing the yield of radiative recombination *via* thermal decays, or providing an alternative radiative relaxation path characterized by shorter lifetimes. Another consequence of a ZnS shell growth is the shift of the photoluminescence band at lower wavelengths. This effect is more pronounced with respect to Cd-based type I core–shell QDs (*e.g.*, for CIS/ZnS core/shell, the blue shift is 130 nm compared to the CIS emission, Δ = 335 meV) and it is associated to the interdiffusion of Zn^{2+} into the core or a cation exchange.[103] Absorption and emission spectra can also be tuned in the Vis/NIR range by alloying CIS QDs with other semiconductors and elements, including Ag, Al and Zn (Fig. 6).[42,104–106]

Despite the fact that the luminescence spectrum of CIS QDs is compatible with the biological window – the emitted photons are thus able to penetrate tissues – the excitation could represent a considerable problem for the detection *in vivo*. As a matter of fact, the molar absorption coefficient of CIS QDs is high for high energy photons (>3.5 eV), which are, however, absorbed by the tissues, while it is quite low for red to NIR photons (<2 eV), which could provide a better tissue penetration.[37,39] A solution to this issue could be offered by non-linear optical phenomena such as two-photon absorption (2PA): this technique consists in the excitation of a chromophore with two simultaneous photons each with half energy than the photons used for the conventional excitation (Fig. 7) and it has been demonstrated suitable for CIS QDs.[63,89,107–109] The absorption cross-section (σ_2) was evaluated for different sized QDs:[107] for instance, 3.0 nm-sized CIS QDs displayed a σ_2 value at 1050 nm equal to 9.3×10^{-48} cm^4 s, or 930 Goeppert–Mayer units; larger nanoparticles possess a higher cross-section. Surely, NIR excitation provides some advantages: an increased depth of imaging and a lower risk of photodamage of the tissues. In addition, excitation with two-photons provides an anti-Stokes emission (*i.e.*, two-photon excited photoluminescence) which further increases the signal-to-noise ratio, because it prevents the excitation of the chromophores naturally present in the biologic matrix and therefore their emission (the so-called autofluorescence).

4. Bioimaging applications

Toxicity and biodistribution

The elements composing CIS QDs show quite different toxicity. Despite that copper(I) can induce reactive oxygen species (ROS) generation,[110] it is considered to be safer than cadmium and lead. Some concerns arise from its disposal, due to its harmfulness for various aquatic environments.[39,111] The toxicity of indium compounds has been extensively studied, especially because of the use of its radioactive isotopes for nuclear medicine. Ionic indium has shown toxicity on kidneys, showing tubular necrosis, and at high concentrations focal necrosis in the liver. Hydrated indium oxides, probably due to their insolubility and consequent phagocytosis, have shown a higher toxicity, especially on reticuloendothelial system, and they are known to be accumulated in the liver, spleen and bone marrow, causing focal necrosis.[112,113] Indium oxide nanoparticles are known to induce lung intercellular toxicity in rats.[114] A review by Nakajima *et al.* studied the possibility of embryotoxicity and teratogenicity in experimental animals.[115]

 This journal is © The Royal Society of Chemistry 2021

Published on 15 2021. Downloaded on 03.10.2024 13:38:38.

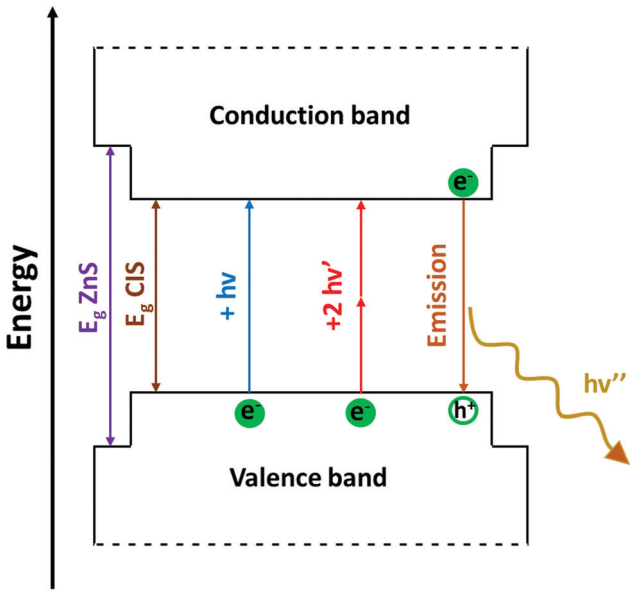

Fig. 7 Schematic representation of the non-resonant two-photon excitation process (red arrows) and two-photon excited luminescence (orange arrow) in colloidal quantum confined $CuInS_2$/ZnS type-I core/shell heterostructures, compared to the classical absorption mediated by one photon (blue arrow). Here, $hv > hv'$.

Concerning the safety of nanoparticles, different factors have to be taken into account, including size, shape and coating.[9] For instance, it is well-known that, generally, smaller nanoparticles (as reported for silica or gold nanoparticles) are considered to be more toxic towards certain cells, probably because of the high surface over volume atoms ratio which overexposes more reactive surface sites.[116–118]

CIS and zinc alloyed CIS (CISZ) QDs are generally considered non-toxic.[35,36,40,41,43] Several studies have reported a high cell-viability for various CIS QDs.[77,119,120] PEGylated CIS/ZnS QDs showed a good biocompatibility and low toxicity *in vivo* in BALB/c mice,[121,122] even though studies related to the over-exposed PEG terminal group (*e.g.* –COOH, $–NH_2$, $–OCH_3$, –OH) should be assessed as reported for other QDs.[123] In a study, Kays *et al.*[124] compared the toxicity of shell-free copper indium sulfide QDs with CIS/ZnS core–shell nanoparticles encapsulated in an amphiphilic lipid–polymer ($DSPE\text{-}PEG_{2k}$). The shell-free nanocrystals induced significant toxicity *in vivo* due to the release of toxic ions, while the ZnS shell prevented the degradation, resulting in a better biocompatible system. Conversely, shell-free and core–shell QDs coated with *O*-carboxymethylchitosan were studied in *Caenorhabditis elegans* models by Chen *et al.*[125] Both the nanoparticles showed a good chemical stability and non-toxicity after exposure times up to 96 h.

In addition to toxicity, pharmacokinetics and accumulation of QDs are paramount. FDA requires that all injected contrast agents should be excreted from the body in a reasonable time. Bioaccumulation in spleen and thymus of BALB/c mice of PEGylated CIS/ZnS QDs with a high hydrodynamic diameter (*ca.* 17 nm) was reported by Chen *et al.* after a period of 28 days.[122] Conversely, biodistribution of non-PEGylated nanocrystals was assessed by Li *et al.*[71] In this study, CIS/ZnS QDs were synthesized in organic phase and then transferred into water by ligand exchange with DHLA. The nanoparticles were injected intravenously into the tail of nude mice and the biodistribution was assessed by fluorescence reflectance imaging. 24 hours after the injection, the nanoparticles were localized mainly in the lungs (which are known to act as a filter for capillary blood fluxes) and the organs of the reticuloendothelial system (liver and spleen). This is probably due to the negatively charged surface of DHLA-CIS/ZnS QDs which cannot prevent the opsonization.[126] The resulting nanoparticles assume a higher hydrodynamic volume due to the adsorbed proteins and consequently are directed to the liver or spleen to be degraded and excreted. This implies the necessity of a short PEGylation or a zwitterionic coating maintaining a low hydrodynamic volume (inferior to *ca.* 5 nm, *i.e.* the cutoff threshold filter in kidneys) in order to permit a rapid renal excretion.

Bioimaging

Bioimaging is defined as the ensemble of techniques used to acquire, process and visualize structural or functional images of living objects or systems at a molecular level.[127] It can operate on cell lines (*in vitro*) or in a body (*in vivo*). Several well-known bioimaging techniques are magnetic resonance imaging (MRI), positron emission tomography (PET), computed tomography (CT), ultrasound (US), optical imaging (OI), *et cetera*.

In OI, the light is the investigational tool; luminescence (or fluorescence) imaging is a particular type of OI in which the emitted light from a contrast agent present in a tissue or organ is detected in order to accomplish the diagnosis.[128–131] It represents a very interesting bioimaging technique, due to its low cost and short acquisition time. For their peculiar optical properties, QDs, and in particular CIS QDs, have been widely considered for luminescence imaging.

Tumor targeting

An undoubted benefit of nanoparticles over molecular probes is the possibility to be conjugated with specific binders for certain tumor cells. This allows the so-called active targeting: the injected nanoparticles are directed towards the specific tumor site due to the favorable interaction between the functionalizing molecule and the receptor overexpressed onto the cells.[132] This allows a high degree of specificity both *in vitro* than *in vivo* and various examples are reported for CIS QDs.

Foda *et al.*[77] demonstrated that CIS/ZnS core–shell systems embedded in a silica shell ($CIS/ZnS@SiO_2$) can be used for cell imaging *in vitro*. The bright red emitting nanoparticles were bio-conjugated with holo-Transferrin (Tf) and were incubated with HeLa cells, which are known to overexpress appropriate receptors. After an incubation period of 12 h and purification *via* PBS washing, UV excitation was used to reveal the red/NIR emission of the adsorbed nanoparticles (Fig. 8a), showing a successful recognition. A sample of Tf-free CIS/ZnS QDs embedded in a silica shell was used as control and a low signal was detected after incubation (Fig. 8b). Moreover, no

Published on 15 2021. Downloaded on 03.10.2024 13:38:38.

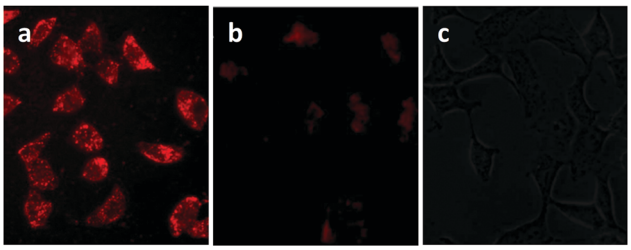

Fig. 8 (a) Luminescence imaging of HeLa cells incubated with CIS/ZnS@SiO_2@Tf nanoparticles under UV excitation; the control experiment of (b) HeLa cells incubated with CIS/ZnS@SiO_2 QDs for 12 h, (c) HEK 293 cell line incubated with CIS/ZnS@SiO_2@Tf for 12 h. Adapted with permission from ref. 77. Copyright (2014) American Chemical Society.

photoluminescence was detected for Tf-conjugated nanoparticles with cells exposing limited Tf receptors (*e.g.* HEK 293 cell line), highlighting that such systems can be used for targeted cellular imaging (Fig. 8c).

Another example of *in vitro* bioimaging was given by Zhao *et al.*[133] CIS/ZnS were transferred in aqueous environment *via* ligand exchange with firstly mercaptopropionic acid and finally glutathione. They were subsequently incubated in MCF10CA1a breast tumor cells in Petri dish and the emitted light was detected with a confocal microscope. The outcomes showed that the nanoparticles successfully stained preferentially the cytoplasm or the perinuclear area than the nuclei.

Deng *et al.*[98] synthesized different sized, and therefore different emitting, CIS/ZnS QDs and embedded them in a chitosan-micelle modified with folate (FA). *In vitro* imaging of folate-receptor positive Bel-7402 tumor cells was successfully reported, and the authors enounced the advantages with respect to organic fluorescent probes, including chemical stability. The same nanoparticles were also tested *in vivo* in mice, showing an accumulation in FA-receptor positive tumor cells and in the liver (Fig. 9). The presence in the RES organ could be due to the high hydrodynamic volume given by the micelle, as previously explained. The same authors, exploiting the different emissions of the studied QDs, showed the possibility to discriminate between different signals by interposition of suitable cutoff filters.

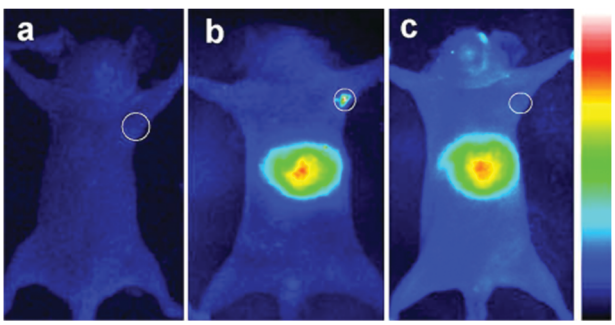

Fig. 9 NIR luminescence images of tumor-bearing mice after intravenous injection with 800 nm emitting CIS/ZnS QDs loaded FA-chitosan micelles for 4 h: (a) before tail-vein injection, (b) FA receptor-positive Bel-7402 tumor-bearing nude mouse, (c) control: FA receptor-negative A549 tumor-bearing nude mouse. The tumor site is indicated by the white circle. Reprinted with permission from ref. 98. Copyright (2012) American Chemical Society.

Other active targeting systems for tumor detection *in vitro* and *in vivo* were explored, indicating the high level of versatility of those nanocrystals. Folic acid-conjugated CIS/ZnS QDs were used to tag and display pancreatic tumor cells in mice by Prasad *et al.*;[109] antibodies conjugated CIS/ZnS QDs passivated with a mixture of 11-mercaptoundecanoic acid and DHLA were assessed for the visualization of BxPC3 pancreatic or U87 MG brain cancer cells.[134] Recently, Niu *et al.*[88] reported a high specificity of CIS/ZnS QDs conjugated with Lys-Pro-Val tripeptide (KPV) for colorectal cancer cells. CIS/ZnS QDs biomineralized in presence of an enzyme were conjugated with IgG antibodies to tag and display THP-1 leukemia cells overexpressing the epidermal growth factor receptor.[68]

All these results are collected in Table 1.

It is interesting to notice that due to the higher biocompatibility of core–shell systems with respect to the shell-free nanoparticles,[124] mostly CIS/ZnS QDs were examined. However, it is well-known that the growth of ZnS shell causes a strong blue-shift to the photoluminescence with respect to the $CuInS_2$ nanocrystal alone, probably due to the interdiffusion of zinc ions into the CIS core or cation exchange with copper(I) ions.[39] Therefore, in order to obtain red emitting nanoparticles, the size of the core should be further increased. This could be an issue for *in vivo* bioimaging applications which request low hydrodynamic volumes and high emission wavelengths.

The problem can be overcome by tuning the composition of the core. By increasing the ratio Cu/In, the emission is shifted towards higher wavelengths, maintaining the same dimensions.

Choi *et al.*[135] demonstrated the use of CIS/ZnS QDs with different cation stoichiometry for *in vivo* imaging, highlighting that the best tissue penetration was achieved for copper-rich QDs (Fig. 10). In addition, the control over the temperature during the ZnS shell growth is a way to avoid the cation exchange.[83]

Another solution could be offered by alloyed systems: doping the core with zinc ions during the core synthesis seems to hinder the cation exchange and red/NIR photoluminescence is preserved. Guo *et al.*[75] exploited this process to obtain CISZ/ZnS QDs with inhibited blue-shift photoluminescence for tumor targeted bioimaging. The nanoparticles were transferred into water by polymer coating and then coupled with Arg-Gly-Asp (cRGD) peptides, which gave selectivity towards U87 MG tumors in mice (Fig. 11).

In addition to active targeting, tagging tumors can be performed by exploiting the enhanced permeation and retention (EPR) effect. Due to their high metabolic activity, tumors usually generate blood vessels that drain the nutrition from the vascular system of the host, in a process called angiogenesis. The newly generated vessels are leaky, so that the drainage can be more efficient. In this way, the circulating agents, among which the nanoparticles, can extravasate more easily in the tumor. This is the basis for the so-called passive targeting.[132,136] Fig. 12 shows the difference between the two types of tumor targeting. In this case, modifications of the surface like PEGylation are required, in order to lower the recognition of the nanoparticles by the RES and enhancing the circulation time of the nanoparticle. An example of these systems was given by Guo *et al.*[66] who reported also a better

 This journal is © The Royal Society of Chemistry 2021

Published on 15 2021. Downloaded on 03.10.2024 13:38:38.

Table 1 Summary of the copper indium sulfide-based nanoparticles, the functionalization and bioconjugation, for bioimaging applications

Nanoparticles	Functionalization	Conjugation	Biomedical application	Ref.
		***In vitro* and *in vivo* imaging of cancer cells**		
CIS/ZnS	Encapsulation in silica matrix	Holo-transferrin	*In vitro* targeted imaging of HeLa tumor cells	Foda *et al.*[77]
CIS/ZnS	Glutathione	—	*In vitro* MCF10CA1a breast tumor cells imaging	Zhao *et al.*[133]
Zinc alloyed CIS/ZnS	Glutathione	Rabbit antibody anti-AFP	*In vitro* targeted imaging of Hep-G2 liver cancer cells	Jiang *et al.*[67]
CIS/ZnS	Encapsulation in a chitosan-micelle	Folic acid	*In vitro* and *in vivo* targeted imaging of Bel-7402 tumor cells	Deng *et al.*[98]
CIS/ZnS	Encapsulation in phospholipide-micelle	Folic acid	*In vivo* imaging of pancreatic tumor cells	Prasad *et al.*[109]
CIS/ZnS	Dihydrolipoic acid	2A3 antibodies	*In vitro* imaging of BxPC3 pancreatic cancer cells	Yu *et al.*[134]
CIS/ZnS	Mercaptopropionic acid	EG2 antibodies	*In vivo* imaging U87 MG brain cancer cells	Yu *et al.*[134]
CIS/ZnS	Encapsulation in (Poly Acrylic Acid)-*n*-octylamine micelle	Lys-Pro-Val tripeptide	*In vitro* and *in vivo* imaging of colorectal Caco-2 tumor cells	Niu *et al.*[88]
CIS/ZnS	Stabilization by L-cysteine	Antibodies 151-Ig	*In vitro* targeted imaging of THP-1 leukemia cells	Spangler *et al.*[68]
CIS/ZnS	Encapsulation in bovine serum albumine - poly(ε-caprolactone)	Arg-Gly-Asp peptides	*In vitro* and *in vivo* targeted imaging of U87 MG tumor cells	Liu *et al.*[175]
Zinc alloyed CIS/ZnS	Encapsulation in poly(maleic anhydride-*alt*-1-octadecene)	Arg-Gly-Asp peptides	*In vivo* targeted imaging of U87 MG tumor cells	Guo *et al.*[75]
Zinc alloyed CIS/ZnS	Encapsulation in poly(maleic anhydride-*alt*-1-octadecene)	—	Time-gated detection of SK-BR-3 breast cancer cells *in vitro*	Mandal *et al.*[154]
		***In vivo* tracking and visualization of tissues**		
Zinc alloyed CIS/ZnS	6-sulfanyl-1-hexanol	—	*In vivo* imaging of RES organs	Guo *et al.*[84]
CIS/ZnS	Poly(ethylene)glycol or micelle encapsulation	—	Sentinel lymph node tracking	Pons *et al.*[86]
$CuInSe_xS_{2-x}$/ZnS	Encapsulation in poly(lactic-*co*-glycolic acid)	Protein invasin	Intestinal M cells tracking	Panthani *et al.*[150]
		Multi-modal imaging		
CIS/ZnS	Mercaptopropionic acid, silica-embedded magnetite NPs	—	Luminescence and MR imaging of HepG2 cells *in vitro*	Wang *et al.*[157]
CIS/ZnS	Silica embedding CIS/ZnS and magnetite NPs	Pt(IV) anticancer drug	Luminescence and MR imaging of MCF-7 cells and drug delivery *in vitro*	Hsu *et al.*[158]
Gd(III) doped CIS/ZnS	Encapsulation in PEGylated dextran-stearyl acid lipid vesicles	—	Luminescence and MR imaging of U87 MG tumor cells *in vivo* and *in vitro*	Yang *et al.*[164]
CIS/ZnS	Gd(III) complex	—	Luminescence and MR imaging of HeLa cells *in vitro* and *in vivo*	Yang *et al.*[162]
CIS/ZnS	Encapsulation in poly(maleic anhydridealt-1-octadecene)	Gd(III) complex, folic acid	Luminescence and MR imaging of HeLa, HepG2, MCF-7 cells *in vitro*	Cheng *et al.*[163]
^{64}Cu doped CIS/ZnS	Poly(ethylene)glycol or glutathione	—	Luminescence imaging, PET and CRET *in vitro* and *in vivo* in U87 MG tumor cells	Guo *et al.*[66]
		Theranostics		
CIS	Electrostatic interactions with poly(L-glutamic acid)	Doxorubicin	Drug delivery and visualization of PC3M cell by luminescence imaging *in vitro*	Gao *et al.*[171]
CIS and CIS/ZnS	Encapsulation in a carboxymethylcellulose polymer	Folic acid and doxorubicin	Drug delivery and visualization of breast cancer cells by luminescence imaging *in vitro*	Mansur *et al.*[172]
CIS	Mercaptopropionic acid and MUC1 aptamer	Daunorubicin	Drug delivery and visualization of PC3M cell by luminescence imaging *in vitro*	Lin *et al.*[176]
CIS/ZnS	Mercaptopropionic acid	Aminolevulinic acid	Photodynamic therapy and luminescence imaging of MCF-7 cells *in vitro*	Feng *et al.*[89]
CIS/ZnS	Encapsulation in lipid-functionalized PEG micelles	—	Phototherapy and multi-modal-imaging (luminescence and MSOT) *in vitro* and *in vivo*	Lv *et al.*[173]

internalization into tumor of PEGylated nanoparticles with respect to non-PEGylated QDs.

CIS QDs for biosensing

Copper indium sulfide QDs have been demonstrated to be valid tools not only for bioimaging, but also for biosensing techniques, acting as fluorescent probes. For instance, the decrease or increase of the luminescent signal from the quantum dot can be related to the concentration of a specific analyte.[137–139] For example, it is known that CIS QDs can be quenched in presence of Cu^{2+},[74] providing therefore an on–off sensing of copper(II) ions. Biosensing is pivotal for biomedical purposes, since the presence and amount of a certain molecule in the serum can be associated to a particular disease.[140,141] In some interesting cases, biosensing can be implemented to bioimaging. An example of this was provided by Lin *et al.*[142]

Published on 15 2021. Downloaded on 03.10.2024 13:38:38.

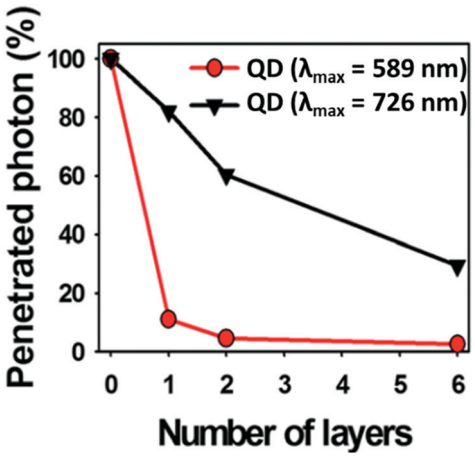

Fig. 10 Photon penetration ratio of CIS QDs with Cu/In = 0.25 and $\lambda_{em\,max}$ = 589 nm (red line) and CIS QDs with Cu/In = 1.8 and $\lambda_{em\ max}$ = 726 nm (black line) using tissue-like phantoms. Adapted from ref. 135 with permission from The Royal Society of Chemistry.

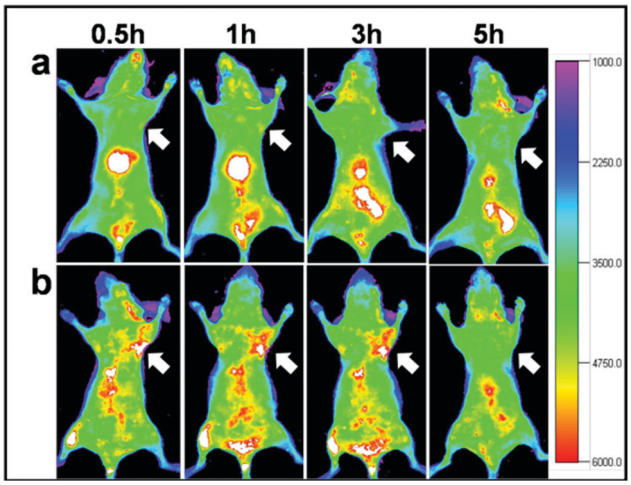

Fig. 11 *In vivo* NIR luminescence imaging of U87MG tumor-bearing mice (arrows) injected with (a) CISZ/ZnS QDs and (b) CISZ/ZnS QDs functionalized with cRGD peptides. The relatively short half-life of the two systems could be due to the rapid uptake by RES, as shown by the accumulation in the liver. Reproduced from ref. 75.

In their work, CIS QDs were synthesized directly in water with mercaptopropionic acid. The system was developed in the presence of Cu^{2+} ions and adenosine-5-triphosphate (ATP). Under these conditions, ATP sequesters copper(II). Acid phosphatases hydrolyzes adenosine-5-triphosphate, liberating the copper(II) ions that quench CIS QDs photoluminescence. Since the enzyme phosphatase has been observed to be produced at higher concentrations in the presence of certain tumors (*e.g.* prostate cancer), acting as biomarker,[143] the studied nanoparticles were utilized *in vitro* on different cell lines to be assessed as probes. The cells containing more phosphatase (in the present case, prostate cancer cells) showed an inferior luminescence from the quantum dots with respect to the control sample.

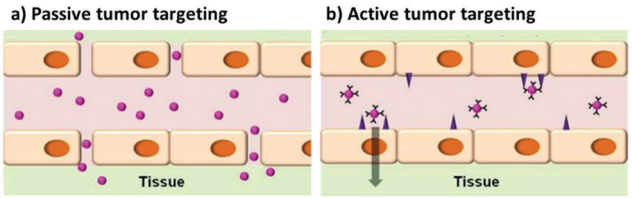

Fig. 12 Scheme representing the concepts between passive and active targeting of tumor cells by quantum dots. Adapted with permission from ref. 136. Copyright (2014) American Chemical Society. DOI: 10.1021/nn500136z.

The sensing of temperature is crucial for studying biological activities in cells and tissues. In this context, the emission quantum yield of the contrast agent is correlated to the temperature in the microenvironment. This could be useful, for instance, to assess cellular activities, hyperthermia monitoring or thermal therapies. CIS QDs encapsulated in micelles were developed by Zhang *et al.*[144] and employed as intracellular temperature-sensitive probes. The nanoparticles were engulfed into HeLa cells and the temperature increased, showing a consistent decrease in the NIR emission of the nanoparticles declared equal to 2.0% $^{\circ}C^{-1}$. The experiments were replicated also *in vivo*, in tumor-bearing mice, injecting the nanoparticles intravenously. By locally increasing the temperature, the photoluminescence recorded from the nanoparticles in the tumor was gradually lower, displaying a declared sensitivity superior to other *in vivo* temperature-sensing systems. The decay was described by the authors as linearly dependent from the temperature. Despite this represents a promising area of research, it should be noticed that both the cited works are based on the variation of the emission intensity of the QDs, which is, however, not reliable, because of the difficulty to quantify the number of absorbed photons by the probe, the scattering of the excitation and emitted light, and the re-absorption of the emitted light. We suggest that future works should rely on the variation of the emission lifetimes, which are more trustworthy for *in vivo* applications.[145]

Sentinel lymph node and vaccine tracking

Apart from tumor targeting, also sentinel lymph node (SLN) tracking is important for the monitoring of the evolution of several kinds of cancer, including melanoma or breast cancer, that spread through lymphatic vessels. This technique consists in the identification of the first lymph node in proximity of the tumor, its resection and analysis. If the presence of tumor cells in the SLN is revealed, it means that the tumor has already spread, and the therapy should be adapted accordingly.[146,147] Nanoparticles with a diameter comprised between indicatively 10 and 50 nm are considered to possess the right size for staining SLNs, being able to reach the lymph node through the afferent lymphatic vessel and to be retained.[148] In addition, a negatively charged surface is preferable, due to the rapid uptake and excellent holding in the lymph node.[149] In this context, Pons *et al.*[86] prepared CIS/ZnS QDs with hydrophobic ligands and transferred them in water by ligand exchange with

 This journal is © The Royal Society of Chemistry 2021

Published on 15 2021. Downloaded on 03.10.2024 13:38:38.

poly(ethylene)glycol or micelle encapsulation. The nanoparticles were administered to mice by subcutaneous injection in a paw. NIR fluorescence imaging (exciting at 690 nm) was performed to visualize two regional LNs corresponding to right axillary lymph nodes 15 minutes after the injection. The nanoparticles accumulated in the region of interest for up to 7 days.

Interestingly, in the same study, detection limit was assessed to 2 pmol injected doses, while inflammation was recorded for an administration of 100 pmol. The results were compared to cadmium-based QDs, which induced the inflammation with a dose of 10 pmol, highlighting the clear difference in toxicity between the two nanomaterials.

A system based on $CuInSe_xS_{2-x}$/ZnS QDs was also studied by Panthani *et al.* to track the movements of orally administered particles (such as oral vaccines).[150] The nanocrystals were encapsulated in poly(lactic-*co*-glycolic) acid microparticles and conjugated with a protein "invasin" specific for intestinal M cells. M cells represent a barrier for pathogens like viruses and bacteria, mediating immune response. They sample the material present in the intestine and deliver it to underlying lymphocytes. Because the access to these lymphocytes is paramount for the absorption of vaccines that are orally administered, tagging M cells could represent a good strategy for oral vaccine delivery.[151] The NIR imaging proved the efficient localization of orally injected invasin-conjugated QDs in the gastrointestinal tract of mice up to 2 days.

Time-gated detection imaging techniques

The visualization of biological tissues through steady-state luminescence imaging usually suffers from a low sensitivity. As a matter of fact, the back-scattered excitation light and the autofluorescence due to the organic fluorophores naturally present in the biological matrixes may enhance the noise. The utilization of $CuInS_2$-based QDs provides a solution, thanks to their long emission lifetimes (hundreds of nanoseconds) if compared to organic fluorophores (units nanoseconds). This can enable time-gated detection (TGD) imaging techniques. Time-gated detection consists in delaying the detection of the emitted light of the biological sample from the excitation pulse, so that the short-lived emitting components of the biological environment are not emitting anymore, while the luminescence of the long-lived components (CIS QDs) is still present. In other words, the recorded light will be due mostly to the $CuInS_2$-based QDs, as explained by Fig. 13. While the integrated optical setup to perform time-gated detection is relatively simple, this results in an enhancement of the signal-to-noise ratio.[152,153] Applications of time-gated detection to *in vitro* bioimaging were given by Mandal *et al.*[154] Zinc alloyed CIS/ZnS QDs were encapsulated in an amphiphilic polymer and used to tag SK-BR-3 breast cancer cells. The cells were subjected to a 10-ns time-gated detection bioimaging. Autofluorescence (lifetimes of *ca.* 1.5 ns) was successfully suppressed (Fig. 14), improving the signal-to-noise ratio by one order of magnitude with respect to steady-state detection. In addition, the system was studied with fluorescence lifetime imaging microscopy (FLIM), *i.e.* a microscopy technique that discriminates by color different emitters depending on their lifetime. A comparison with CdSe/ZnS QDs (lifetime of 8.24 ns) and Alexa488 fluorophore (with lifetime slightly longer than autofluorescence) tagging the same cells was performed revealing the suitability of CIS QDs for time-gated detection imaging techniques.

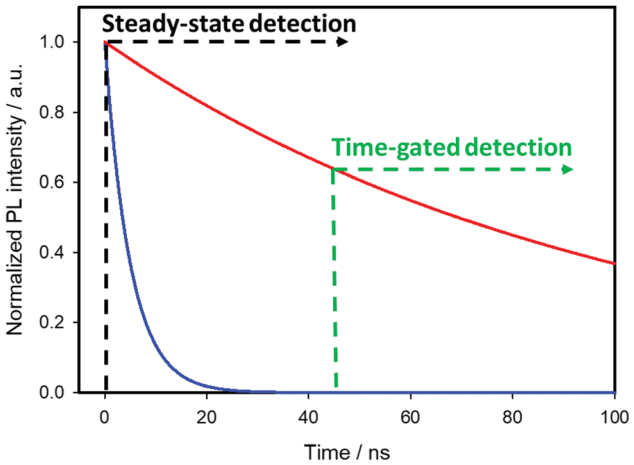

Fig. 13 Comparison between steady state (or continuous) detection and time-gated detection. A continuous detection from the excitation pulse at time = 0 includes the emission of short-living components (whose decay in time is represented by the mono-exponential solid blue line, τ_{blue} = 5 ns) and long-living ones (red line, τ_{red} = 100 ns). A delayed detection suppresses the first ones.

Multi-modal imaging

One of the most fascinating features of nanotechnology is the possibility to allow multi-modal imaging by combining in the same nanoparticle contrast agents specific for different diagnostic techniques.[155,156] This is useful to circumvent the problems related to the use of just one technique, *e.g.* the sensitivity, the tissue penetration, the spatial resolution, *et cetera*. One example consists in coupling QDs useful for luminescence imaging with paramagnetic ions used as contrast agents for magnetic resonance imaging (MRI). Among them, iron oxide-containing nanoparticles[2,3] or lanthanide complexes[155] have been extensively studied for their magnetic behavior.

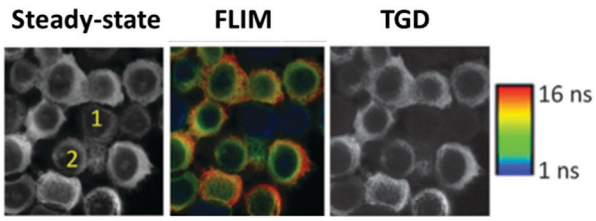

Fig. 14 On the left, steady-state luminescence intensity images with two cells labeled 1 (receptor free, highly autofluorescent) and 2 (overexpressing receptor Her2) whose membrane is stained with Her2-specific CIS QDs; in the middle, FLIM images; ranging from 1 ns (blue) to 16 ns (red); on the right side, image after time-gating the first 10 ns of photons significantly improving contrast, and removes unlabeled cells from the images. Reproduced from ref. 154 with permission from The Royal Society of Chemistry.

Published on 15 2021. Downloaded on 03.10.2024 13:38:38.

Their contrast enhancement is due to a modification of the relaxation times (longitudinal or transverse) of the protons of water in the proximity. Conjugation of CIS QDs with paramagnetic ions has been mainly accomplished by three different ways: integration with iron oxide nanoparticles,[157,158] doping with Gd(III) or Mn(II) ions,[62,159–161] and functionalization with Gd(III) complexes.[162,163] Wang *et al.*[157] prepared magnetic $CuInS_2$/ZnS nanocrystals by integrating silica-embedded magnetite nanoparticles with mercaptopropionic acid modified CIS/ZnS QDs, showing both superparamagnetic and photoluminescence properties. Alloying the nanoparticle with lanthanide ions, for instance, was accomplished by Yang *et al.*[164] Gd(III) was incorporated into CIS/ZnS during the core synthesis. The nanoparticles were transferred into water after encapsulation in PEGylated dextran-stearyl acid polymeric lipid vesicles. *In vitro* and *in vivo* experiments were performed to display pronounced longitudinal relaxivity (r_1 = 9.45 mM^{-1} s^{-1}). Doping with paramagnetic ions, however, usually worsens the photoluminescence properties. Yang *et al.*[162] developed bimodal contrast nanoagents based on CIS/ZnS functionalized *via* ligand exchange with 2-[bis[2-[carboxymethyl-[2-oxo-2-(2-sulfanylethyl-amino)ethyl]amino]ethyl]amino] acetic acid (DTDTPA). Afterwards this chelates Gd(III) ions, yielding CIS QDs functionalized with gadolinium complexes. MRI was studied *in vitro* on HeLa cells and *in vivo* in tumor-bearing mice (Fig. 15a). MR intensity was observed to increase in 24 h post injection in the tumor site, assessing its bioaccumulation *via* passive targeting (Fig. 15b). The longitudinal relaxivity was recorded to be 2.5 times higher than the already approved molecular probe based on DTPA gadolinium complex. Also, photoluminescence was recorded *in vivo*, highlighting the ability to display both optical and magnetic resonance imaging. Apart from lanthanides and elements with a high number of unpaired electrons for magnetic resonance imaging, QDs can be implemented with radionuclides, which can accomplish diagnostic techniques based on nuclear medicine, namely Positron Emission Tomography (PET), Single Photon Emission Computed Tomography (SPECT), Cerenkov Luminescence Imaging (CLI).[5] In particular, CLI has emerged only in the last decade, providing both an interesting and cheap investigational tool *in vivo* and also dosimetry information during diagnosis or therapies that exploit radiopharmaceuticals.[165] It allows the visualization of radiotracers that emit Cerenkov Radiation (CR). CR is an electromagnetic wave generated when charged nanoparticles moves in a medium faster than the speed of light in the same dielectric. It is associated to nuclear medicine because the charged nanoparticles are usually generated by nuclear decays (especially negatron β^- and positron β^+ emitters) or by external high energy irradiation (linear accelerators, X-ray sources).[166] Unfortunately, the CR emission is more intense at UV-blue spectral range, which is unsuitable for *in vivo* imaging, as previously discussed.[167,168] CIS QDs can provide a solution. Their absorption spectra overlap well with the CR emission. In these circumstances, a process called Cerenkov resonance energy transfer (CRET) can take place: the radionuclide sensitizes CIS QDs, thus converting the blue Cerenkov radiation in most penetrating red/NIR photons. It is worth noting that this process does not require excitation light, which usually limits the application of bioimaging due its poor tissue penetration. Similar systems were described by Guo *et al.*[66] Positron emitter ^{64}Cu was incorporated into CIS/ZnS nanocrystals during the core formation, providing intrinsically radioactive QDs (RQDs). The colloidal stability in aqueous environment was provided by a functionalization of the surface with poly(ethylene)glycol or glutathione (GSH). Firstly, CRET occurrence from the β^+ emitter to the QD was successfully verified by *in vitro* analysis (Fig. 16a): in absence of external stimuli, the sample containing RQDs emitted red light, while the control containing just a ^{64}Cu salt showed the typical blue CR emission. Therefore, the nanoparticles were tested *in vivo* in mice bearing human U87 glioblastoma tumor (Fig. 16b). The mice were imaged 6 hours post injection with open or 590 nm cutoff filter. Pegylated RQDs showed a higher bioaccumulation in the tumor with respect to ^{64}Cu salt and glutathione functionalized RQDs, probably due to EPR effect. Also, a superior luminescence was recorded both in absence and in presence of red-light filter, assessing the efficiency of CRET. In the same work, the authors proved the possibility to perform multi-modal imaging, coupling positron emission tomography with the conventional optical imaging.

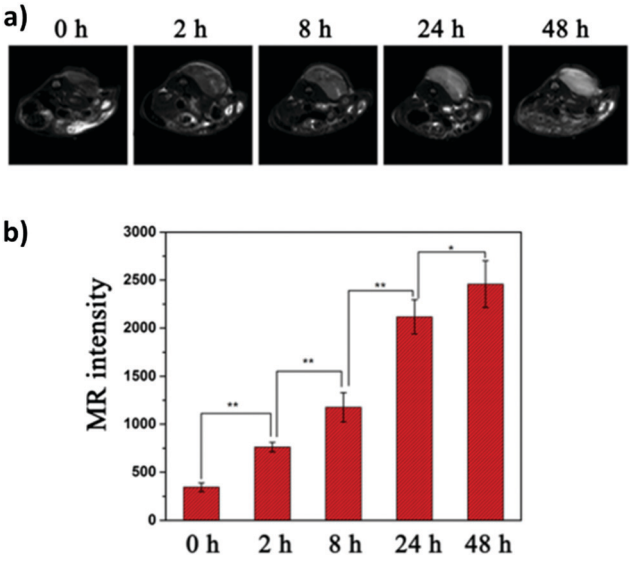

Fig. 15 *In vivo* longitudinal relaxation time-weighted MR images (a) and MR signal intensities (b) of HeLa-bearing nude mice at 0, 8, 24, and 48 h after tail vein injection of Gd chelate CIS QDs. Adapted with permission from ref. 162. Copyright (2017) American Chemical Society.

Theranostics

The rise of nanotechnology in medicine has allowed to integrate diagnostic and therapeutic tools in the same system, enabling the so-called theranostics.[169] Despite the development of this field is still at an early stage, there are potential benefits with respect to the conventional therapeutics, including a real-time evaluation of the therapy and assessment of treatment efficacy.[170] Various examples are reported for CIS QDs. Gao *et al.*[171] proved the efficiency of doxorubicin (DOX) conjugated

 This journal is © The Royal Society of Chemistry 2021

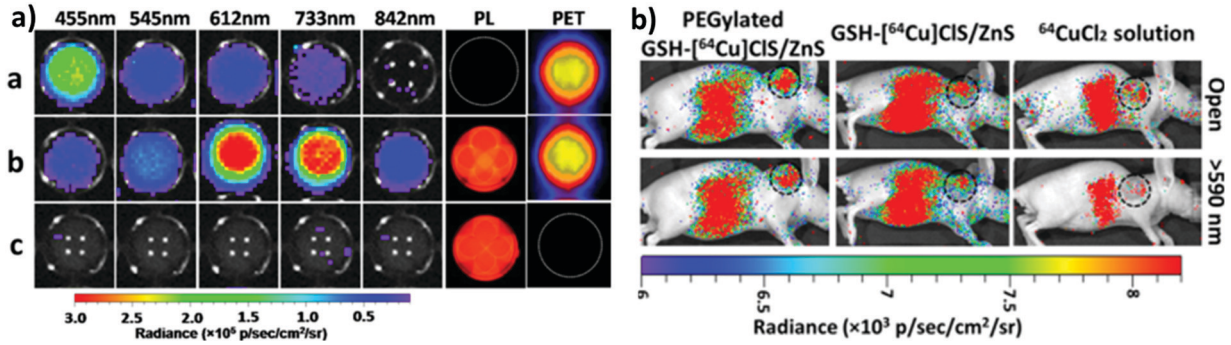

Fig. 16 (a, left) PET, photoluminescence (PL) and CRET luminescence images derived with various narrow filters for the $^{64}CuCl_2$ (a, 150 μCi), [^{64}Cu]CIS/ZnS RQDs (b, 150 μCi, 25 μg),and CIS/ZnS nonradioactive QDs (c, 25 μg) aqueous solutions, respectively. The CRET luminescence images were acquired with acquisition time of 4 min. The PL images were obtained under blue excitation light with exposure time of 0.1 s. (b, right) CRET images of U87 MG tumor-bearing mice at 6 h post injection of 100 μL (300 μCi) of $^{64}CuCl_2$, glutathione-[^{64}Cu]CIS/ZnS and PEGylated [^{64}Cu]CIS/ZnS RQDs, respectively. Circle, tumor area. These luminescence images were acquired without excitation light with open and red filter (>590 nm). Adapted with permission from ref. 66. Copyright (2015) American Chemical Society. DOI: 10.1021/nn505660r.

Published on 15 2021. Downloaded on 03.10.2024 13:38:38.

CIS QDs for the simultaneous imaging and treatment of cancer cell *via* drug delivery. In particular, positive charged CIS QDs were conjugated by electrostatic interactions with negatively charged poly(L-glutamic acid) (PGA) functionalized with the anticancer drug DOX. In this complex, the emission of the QD is quenched by photoinduced electron transfer to DOX. After incubation in cancer cells, PGA is hydrolyzed, resulting in the release of DOX and separation from CIS QDs. The nanocrystals recover their emission, and the photoluminescence intensity can be correlated to the amount of liberated DOX, providing a tool for monitoring the drug release in the cancer cells. Cytotoxicity studies in tumor cells *in vitro* confirm the reduced viability due to DOX conjugated CIS QDs with respect to DOX-free QDs (Fig. 17). Another recent example involving CIS QDs for drug delivery was given by Mansur *et al.*[172] CIS/ZnS QDs were directly synthesized in water stabilized by a carboxymethylcellulose (CMC) biocompatible polymer. Folic acid (FA) was then linked *via* amide coupling and DOX was conjugated *via* non-covalent interactions. Therefore, incubation of free DOX anticancer drug, non-conjugated CIS/ZnS QDs and DOX + FA-conjugated CIS/ZnS QDs was performed on different kinds of cells: cancer cells overexposing folate receptor, cancer cells in absence of folate receptor and healthy cells. Non-conjugated QDs did not display cytotoxicity. Free DOX caused a decrement of viability in all the cell samples. DOX + FA-conjugated CIS/ZnS QDs caused a superior toxicity on cells overexpressing FA receptor, probably promoted by a better internalization. The emissions of FA, DOX and CIS/ZnS QDs after endocytosis were used to image the cells.

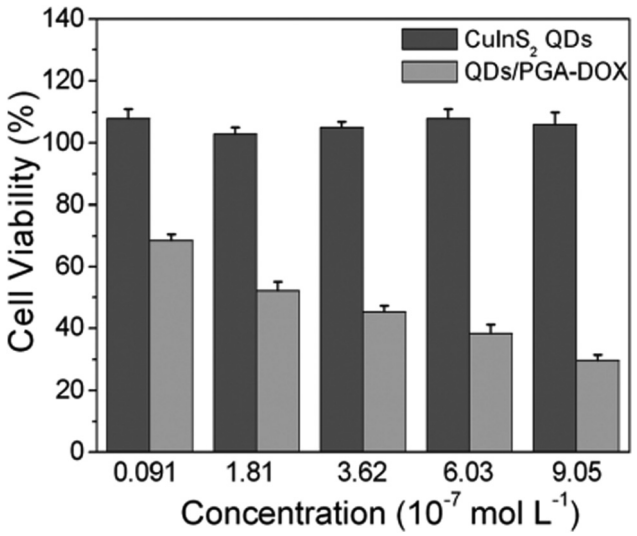

Fig. 17 *In vitro* cell viability of PC3M cells treated with varying concentrations of $CuInS_2$ QDs and DOX-conjugated CIS QDs for 48 h. Percentage cell viability of the treated cells was calculated relative to that of untreated cells (with arbitrarily assigned 100% viability). Reproduced from ref. 171 with permission from The Royal Society of Chemistry.

$CuInS_2$/ZnS QDs were finally assessed as "all-in-one" nanomedicines displaying bi-modal imaging and phototherapy applications by Lv *et al.*[173] Multi-modal imaging was accomplished by combining the typical NIR luminescence imaging with multispectral optoacoustic tomography (MSOT). MSOT allows to overcome the limitations of optical diffusion with the spatial resolution of ultrasound detection generated by photoacoustic effect (PA). In principle, pulsed light of short duration is used to excite the sample that produces acoustic waves. Those photoacoustic waves are collected to generate an image. In contrast with conventional PA techniques, MSOT relies on spanning various excitation wavelengths, allowing to differentiate the chromophores, *e.g.* hemoglobin from nanoparticles.[174] In this work, MSOT behavior of CIS/ZnS QDs was studied for different excitation wavelengths and various concentrations. The authors reported a linear correlation between PA and the concentration of the nanoparticles up to 200 μg mL^{-1}. PA spectrum was also recorded, showing a higher signal for lower excitation wavelengths (<800 nm). Luminescence/MSOT dual-modal imaging was also assessed *in vivo*. CIS/ZnS QDs encapsulated in lipid-functionalized PEG micelles with different hydrodynamic volumes were intravenously injected in tumor bearing mice. NIR luminescence imaging showed an accumulation of CIS QDs in the tumor between 6 and 48 h post injection, due to EPR effect, with a slight decrease after 24 h (Fig. 18a). Therefore, MSOT imaging was

Published on 15 2021. Downloaded on 03.10.2024 13:38:38.

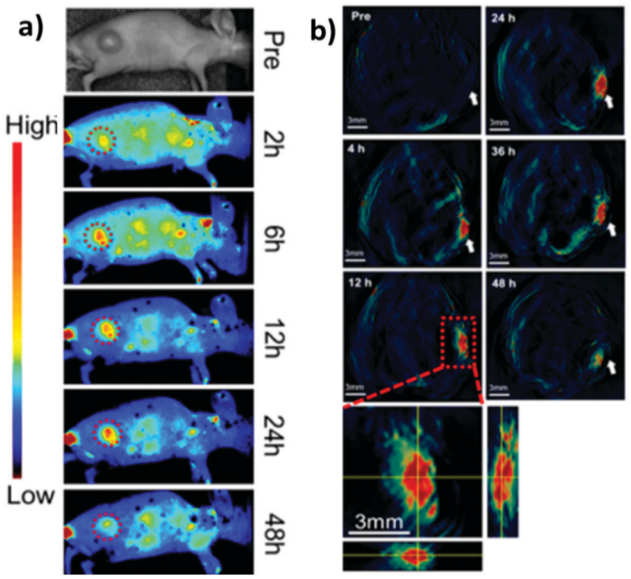

Fig. 18 Comparison between luminescence imaging and MSOT *in vivo*. (a) NIR luminescence images of tumor-bearing mice at various time points after intravenous injections of CIS/ZnS QDs with hydrodynamic diameter of 25 nm. (b) MSOT images of tumors (arrows) in mice taken at different times after intravenous injection of the same CIS/ZnS QDs. Enlarged orthogonal views of the tumor region are also presented. Adapted with permission from ref. 173. Copyright (2016) American Chemical Society.

acquired, providing a higher spatial resolution and better information on the bioaccumulation times (Fig. 18b).

The same nanoparticles were tested for phototherapy applications. The use of light-activated treatments show various advantages, including spatiotemporal selectivity, reduced side effects and minimal invasiveness.[173] Among them, tumor ablations can be performed by photothermal therapy (PTT) and photodynamic therapy (PDT). Photothermal therapy consists in the thermal relaxation of a photoexcited contrast agent. The released heat enhances the temperature of the surrounding tissue (*i.e.* the tumor), causing cell necrosis. In contrast, photodynamic therapy relies in the photoinduced energy transfer from the excited pharmaceutical to dioxygen *in situ*. Oxygen is sensitized at its first singlet excited state, which is known to be cytotoxic and damages the tumoral tissue. Photothermal and photodynamic effects were firstly tested in solution. Continuous irradiation with a 660 nm laser over a period of 10 minutes resulted in an enhancement of the temperature of the solution only in presence of CIS/ZnS QDs. Photostability of the QDs was reported by various heating/cooling cycles. To investigate the generation of singlet oxygen following CIS QD photosensitization, the nanoparticles were suspended in an aqueous solution of *p*-nitrosodimethylaniline (RNO), a species subject to bleaching in presence of reactive-oxygen species. After exposure to the same laser irradiation, a decrease of RNO absorption spectra (maximum at 440 nm) was detected, symptom of the generation of ROS. The nanoparticles were proved to display both the photoinduced effects. Therefore, viability on mouse mammary carcinoma 4T1 cells was tested in presence or absence of irradiation with QDs. During an irradiation period of 10 minutes with 660 nm laser (1 W cm^{-2}) 95% of the cells were killed, in contrast to what happened with the control samples (absence of irradiation or without QDs). This suggested that photoablation occurred, probably due to a combination of both PTT and PDT. Eventually, test *in vivo* in 4T1 tumor-bearing mice were performed. The treated mice were administered CIS/ZnS QDs (40 mg kg^{-1}) and exposed to the same laser irradiation tested *in vitro* after 12 h post injection. Thermal images were continuously acquired in the tumor site, recording a local temperature enhancement to 46 °C after 6 minutes. After the treatment, a decrease in the tumor volume due to the photo-ablation was reported. It is worth noting that both the diagnostic and the therapeutic techniques involve the same excitation light pulse, yielding a potential tool that allows multiple imaging and treatment at the same time.

5. Conclusion and future perspectives

The enormous development of the synthetic methodologies of nanocrystalline semiconductors in the last decades has led to a multitude of technological and biomedical applications. This consideration holds also for CIS QDs (Fig. 19), which, due to their low toxicity, peculiar photophysical properties, and inexpensive production cost have emerged among different kinds of semiconducting nanoparticles as valid tools for *in vivo* and *in vitro* investigations.

We have therefore summarized the main synthetic methods for the production of CIS QDs, their photophysical features and the most recent applications for bio-labelling purposes; although recent progresses show vast and diverse applicability, we are able to underline, in perspective, advantages and potential limitations in their use.

• CIS QDs feature an elevated absorption cross-section, good photostability and a high photoluminescence quantum yield. Their size- and composition-dependent emission matching the biological transparency window and their long lifetimes represent ideal features for their use in biological matrices. Moreover, CIS QDs can overcome several issues from which typical QDs or conventional molecular probes used for bioimaging applications usually suffer, including the suppression of autofluorescence and tissue penetration by two-photon absorption.

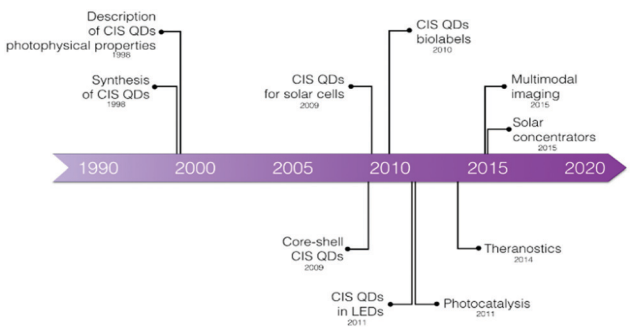

Fig. 19 Historical overview of the CIS quantum dots.

This journal is © The Royal Society of Chemistry 2021

Published on 15 2021. Downloaded on 03.10.2024 13:38:38.

• Concerning their toxicity, CIS QDs have generally been considered suitable entities for the interaction with living cells. The toxicity of isolated ions was also considered, emphasising the need of nanoparticle shelling to reduce the loss of cations in biological tissues. Furthermore, due to the dependence between common nanoparticles toxicities and their size, morphology and terminal groups of the functionalizing moiety, we draw attention to consider cytotoxicity studies on CIS QDs with different dimensions, shapes and overexpressed molecules (*e.g.* the charge and the terminal group in PEGylated nanocrystals). Being biodistribution and bioaccumulation in RES organs important for the administration of contrast agents, further studies should be addressed on nanoparticle-based hybrid systems which could be readily excreted through renal filtration. Hence, the decoration of the particle with charged substituents (for instance, by means of an inorganic ligand exchange or through a zwitterionic functionalization) should be considered for successful developments.

• CIS QDs have displayed very high adaptability for bioimaging applications. Bioconjugation was frequently demonstrated to be an effective way to introduce binders for enabling active targeting of specific cells, although EPR (enhanced permeation and retention) effect was also used to tag tumors. The suitability of the system is ameliorated by taking advantage of the features of the nanocrystals. By employing time-gated detection techniques, CIS QDs emitting in the NIR spectrum are able to enhance the signal-to-noise ratio *in vitro*. In summary, CIS QDs were proved to be appropriate platform for the combination of different imaging techniques (in particular MRI, PET, CRET and MSOT), acting as multi-modal imaging diagnostic tools, even in drug delivery and phototherapy. Also, the implementation of sensing to bioimaging seems to be a compelling application, but, for future works, researchers should rely on the variation of emission lifetimes instead of emission intensity.

Although the research focused on biological applications of copper indium sulfide QDs is relatively recent, it is undoubted that the future of this semiconducting nanomaterial is bright. We hope the collaboration between researchers with different backgrounds – chemistry, biology, nanophysics, and medicine over all – could be consolidated for the realization of useful bioimaging systems and techniques (for example, in light-guided surgery, cancer cells tagging, nanomedicine, *etc.*).

Conflicts of interest

There are no conflicts to declare.

Acknowledgements

The University of Bologna is gratefully acknowledged for financial support. KC thanks the EPSRC (EP/T013753/1) for financial support.

References

1 K. Zarschler, L. Rocks, N. Licciardello, L. Boselli, E. Polo, K. P. Garcia, L. De Cola, H. Stephan and K. A. Dawson, *Nanomedicine*, 2016, **12**, 1663–1701.
2 C. Corot, P. Robert, J. M. Idée and M. Port, *Adv. Drug Delivery Rev.*, 2006, **58**, 1471–1504.
3 S. M. Dadfar, K. Roemhild, N. I. Drude, S. von Stillfried, R. Knüchel, F. Kiessling and T. Lammers, *Adv. Drug Delivery Rev.*, 2019, **138**, 302–325.
4 Y. Liu, K. Ai and L. Lu, *Acc. Chem. Res.*, 2012, **45**, 1817–1827.
5 C. A. Ferreira, D. Ni, Z. T. Rosenkrans and W. Cai, *Angew. Chem., Int. Ed.*, 2019, **58**, 13232–13252.
6 E. B. Ehlerding, P. Grodzinski, W. Cai and C. H. Liu, *ACS Nano*, 2018, **12**, 2106–2121.
7 X. Michalet, F. F. Pinaud, L. A. Bentolila, J. M. Tsay, S. Doose, J. J. Li, G. Sundaresan, A. M. Wu, S. S. Gambhir and S. Weiss, *Science*, 2005, **307**, 538–545.
8 T. Pellegrino, S. Kudera, T. Liedl, A. M. Javier, L. Manna and W. J. Parak, *Small*, 2005, **1**, 48–63.
9 G. Xu, S. Zeng, B. Zhang, M. T. Swihart, K. T. Yong and P. N. Prasad, *Chem. Rev.*, 2016, **116**, 12234–12327.
10 M. El-Sayed, *Acc. Chem. Res.*, 2004, **37**, 326–333.
11 C. Burda, X. Chen, R. Narayanan and M. A. El-Sayed, *Chem. Rev.*, 2005, **105**, 1025–1102.
12 M. Montalti, A. Cantelli and G. Battistelli, *Chem. Soc. Rev.*, 2015, **44**, 4853–4921.
13 Y. Wang, R. Hu, G. Lin, I. Roy and K. T. Yong, *ACS Appl. Mater. Interfaces*, 2013, **5**, 2786–2799.
14 I. V. Martynenko, A. P. Litvin, F. Purcell-Milton, A. V. Baranov, A. V. Fedorov and Y. K. Gun'ko, *J. Mater. Chem. B*, 2017, **5**, 6701–6727.
15 W. E. Bawarski, E. Chidlowsky, D. J. Bharali and S. A. Mousa, *Nanomedicine*, 2008, **4**, 273–282.
16 J. Cheon and J. H. Lee, *Acc. Chem. Res.*, 2008, **41**, 1630–1640.
17 Y. P. Ho and K. W. Leong, *Nanoscale*, 2010, **2**, 60–68.
18 H. K. Jun, M. A. Careem and A. K. Arof, *Renewable Sustainable Energy Rev.*, 2013, **22**, 148–167.
19 L. Qian, Y. Zheng, J. Xue and P. H. Holloway, *Nat. Photonics*, 2011, **5**, 543–548.
20 V. Wood and V. Bulovic, *Nano Rev.*, 2010, **1**, 5202.
21 B. Bajorowicz, M. P. Kobylański, A. Gołąbiewska, J. Nadolna, A. Zaleska-Medynska and A. Malankowska, *Adv. Colloid Interface Sci.*, 2018, **256**, 352–372.
22 S. Silvi and A. Credi, *Chem. Soc. Rev.*, 2015, **44**, 4275–4289.
23 A. Bruneau, M. Fortier, F. Gagne, C. Gagnon, P. Turcotte, A. Tayabali, T. A. Davis, M. Auffret and M. Fournier, *Environ. Toxicol.*, 2015, **30**, 9–25.
24 Y. Su, Y. He, H. Lu, L. Sai, Q. Li, W. Li, L. Wang, P. Shen, Q. Huang and C. Fan, *Biomaterials*, 2009, **30**, 19–25.
25 C. M. Johnson, K. M. Pate, Y. Shen, A. Viswanath, R. Tan, B. C. Benicewicz, M. A. Moss and A. B. Greytak, *J. Colloid Interface Sci.*, 2015, **458**, 310–314.
26 H. S. Choi, W. Liu, P. Misra, E. Tanaka, J. P. Zimmer, B. I. Ipe, M. G. Bawendi and J. V. Frangioni, *Nat. Biotechnol.*, 2007, **25**, 1165–1170.

Published on 15 2021. Downloaded on 03.10.2024 13:38:38.

27 J.-Y. Chang, G.-Q. Wang, C.-Y. Cheng, W.-X. Lin and J.-C. Hsu, *J. Mater. Chem.*, 2012, **22**, 10609–10618.
28 C. J. T. Robidillo and J. G. C. Veinot, *ACS Appl. Mater. Interfaces*, 2020, **12**, 52251–52270.
29 R. Mazzaro, F. Romano and P. Ceroni, *Phys. Chem. Chem. Phys.*, 2017, **19**, 26507–26526.
30 F. Romano, S. Angeloni, G. Morselli, R. Mazzaro, V. Morandi, J. R. Shell, X. Cao, B. Pogue and P. Ceroni, *Nanoscale*, 2020, **12**, 7921–7926.
31 S. Bhattacharjee, I. M. C. M. Rietjens, M. P. Singh, T. M. Atkins, T. K. Purkait, Z. Xu, S. Regli, A. Shukaliak, R. J. Clark, B. S. Mitchell, G. Alink, A. T. M. Marcelis, M. J. Fink, J. G. C. Veinot, S. M. Kauzlarich and H. Zuilhof, *Nanoscale*, 2013, **5**, 4870–4883.
32 J. Fan and P. K. Chu, *Small*, 2010, **6**, 2080–2098.
33 A. W. Verheijen, L. J. Giling and J. Bloem, *Mater. Res. Bull.*, 1979, **14**, 237–240.
34 H. Y. Ueng and H. L. Hwang, *J. Phys. Chem. Solids*, 1989, **50**, 1297–1305.
35 J. Kolny-Olesiak and H. Weller, *ACS Appl. Mater. Interfaces*, 2013, **5**, 12221–12237.
36 X. Bai, F. Purcell-milton and Y. K. Gun, *Nanomaterials*, 2019, **9**, 85.
37 M. Booth, A. P. Brown, S. D. Evans and K. Critchley, *Chem. Mater.*, 2012, **24**, 2064–2070.
38 L. Li, A. Pandey, D. J. Werder, B. P. Khanal, J. M. Pietryga and V. I. Klimov, *J. Am. Chem. Soc.*, 2011, **133**, 1176–1179.
39 A. D. P. Leach and J. E. Macdonald, *J. Phys. Chem. Lett.*, 2016, **7**, 572–583.
40 H. Zhong, Z. Bai and B. Zou, *J. Phys. Chem. Lett.*, 2012, **3**, 3167–3175.
41 N. Tsolekile, S. Parani and M. C. Matoetoe, *Nano-Struct. Nano-Objects*, 2017, **12**, 46–56.
42 S. Y. Yoon, J. H. Kim, E. P. Jang, S. H. Lee, D. Y. Jo, Y. Kim, Y. R. Do and H. Yang, *Chem. Mater.*, 2019, **31**, 2627–2634.
43 Z. Long, W. Zhang, J. Tian, G. Chen, Y. Liu and R. Liu, *Inorg. Chem. Front.*, 2021, **8**, 880–897.
44 L. Wang, Z. Guan and A. Tang, *J. Nanopart. Res.*, 2020, **22**, 28.
45 J. J. M. Binsma, L. J. Giling and J. Bloem, *J. Cryst. Growth*, 1980, **50**, 429–436.
46 D. Pan, L. An, Z. Sun, W. Hou, Y. Yang, Z. Yang and Y. Lu, *J. Am. Chem. Soc.*, 2008, **130**, 5620–5621.
47 H. Y. Ueng and H. L. Hwang, *J. Phys. Chem. Solids*, 1989, **50**, 1297–1305.
48 B. Chen, H. Zhong, W. Zhang, Z. A. Tan, Y. Li, C. Yu, T. Zhai, Y. Bando, S. Yang and B. Zou, *Adv. Funct. Mater.*, 2012, **22**, 2081–2088.
49 X. Shen, E. A. Hernández-Pagan, W. Zhou, Y. S. Puzyrev, J. C. Idrobo, J. E. Macdonald, S. J. Pennycook and S. T. Pantelides, *Nat. Commun.*, 2014, **5**, 1–6.
50 S. T. Connor, C. M. Hsu, B. D. Weil, S. Aloni and Y. Cui, *J. Am. Chem. Soc.*, 2009, **131**, 4962–4966.
51 C. Xia, J. D. Meeldijk, H. C. Gerritsen and C. De Mello Donega, *Chem. Mater.*, 2017, **29**, 4940–4951.
52 H. Zhong, S. S. Lo, T. Mirkovic, Y. Li, Y. Ding, Y. Li and G. D. Scholes, *ACS Nano*, 2010, **4**, 5253–5262.
53 R. Xie, M. Rutherford and X. Peng, *J. Am. Chem. Soc.*, 2009, **131**, 5691–5697.
54 S. L. Castro, S. G. Bailey, R. P. Raffaelle, K. K. Banger and A. F. Hepp, *Chem. Mater.*, 2003, **15**, 3142–3147.
55 S. L. Castro, S. G. Bailey, R. P. Raffaelle, K. K. Banger and A. F. Hepp, *J. Phys. Chem. B*, 2004, **108**, 12429–12435.
56 B. Chen, S. Chang, D. Li, L. Chen, Y. Wang, T. Chen, B. Zou, H. Zhong and A. L. Rogach, *Chem. Mater.*, 2015, **27**, 5949–5956.
57 W. Van Der Stam, A. C. Berends, F. T. Rabouw, T. Willhammar, X. Ke, J. D. Meeldijk, S. Bals and C. De Mello Donega, *Chem. Mater.*, 2015, **27**, 621–628.
58 H. Nakamura, W. Kato, M. Uehara, K. Nose, T. Omata, S. Otsuka-Yao-Matsuo, M. Miyazaki and H. Maeda, *Chem. Mater.*, 2006, **18**, 3330–3335.
59 K. E. Hughes, S. R. Ostheller, H. D. Nelson and D. R. Gamelin, *Nano Lett.*, 2019, **2**, 1318–1325.
60 Y. A. Wang, X. Zhang, N. Bao, B. Lin and A. Gupta, *J. Am. Chem. Soc.*, 2011, **133**, 11072–11075.
61 Q. Liu, Z. Zhao, Y. Lin, P. Guo, S. Li, D. Pan and X. Ji, *Chem. Commun.*, 2011, **47**, 964–966.
62 J. Y. Chang, G. R. Chen and J. D. Li, *Phys. Chem. Chem. Phys.*, 2016, **18**, 7132–7140.
63 X. Tang, W. Cheng, E. S. G. Choo and J. Xue, *Chem. Commun.*, 2011, **47**, 5217–5219.
64 Y. Chen, S. Li, L. Huang and D. Pan, *Inorg. Chem.*, 2013, **52**, 7819–7821.
65 S. Liu, H. Zhang, Y. Qiao and X. Su, *RSC Adv.*, 2012, **2**, 819–825.
66 W. Guo, X. Sun, O. Jacobson, X. Yan, K. Min, A. Srivatsan, G. Niu, D. O. Kiesewetter, J. Chang and X. Chen, *ACS Nano*, 2015, **9**, 488–495.
67 T. Jiang, J. Song, H. Wang, X. Ye, H. Wang, W. Zhang, M. Yang, R. Xia, L. Zhu and X. Xu, *J. Mater. Chem. B*, 2015, **3**, 2402–2410.
68 L. C. Spangler, R. Chu, L. Lu, C. J. Kiely, B. W. Berger and S. McIntosh, *Nanoscale*, 2017, **9**, 9340–9351.
69 W. W. Xiong, G. H. Yang, X. C. Wu and J. J. Zhu, *ACS Appl. Mater. Interfaces*, 2013, **5**, 8210–8216.
70 R. R. Silva, D. V. Freitas, F. L. N. Sousa, A. C. Jesus, S. E. Silva, A. A. P. Mansur, S. M. Carvalho, D. S. Marques, I. C. Carvalho, W. M. Azevedo, H. S. Mansur and M. Navarro, *J. Alloys Compd.*, 2021, **853**, 56926.
71 L. Li, T. J. Daou, I. Texier, T. T. K. Chi, N. Q. Liem and P. Reiss, *Chem. Mater.*, 2009, **21**, 2422–2429.
72 J. Choi, W. Choi and D. Y. Jeon, *ACS Appl. Nano Mater.*, 2019, **2**, 5504–5511.
73 G. Gabka, P. Bujak, K. Giedyk, K. Kotwica, A. Ostrowski, K. Malinowska, W. Lisowski, J. W. Sobczak and A. Pron, *Phys. Chem. Chem. Phys.*, 2014, **16**, 23082–23088.
74 M. Booth, R. Peel, R. Partanen, N. Hondow, V. Vasilca, L. J. C. Jeuken and K. Critchley, *RSC Adv.*, 2013, **3**, 20559–20566.
75 W. Guo, N. chen, Y. Tu, C. Dong, B. Zhang, C. Hu and J. Chang, *Theranostics*, 2013, **3**, 99–108.

 This journal is © The Royal Society of Chemistry 2021

Published on 15 2021. Downloaded on 03.10.2024 13:38:38.

76 E. S. Speranskaya, N. V. Beloglazova, S. Abé, T. Aubert, P. F. Smet, D. Poelman, I. Y. Goryacheva, S. De Saeger and Z. Hens, *Langmuir*, 2014, **30**, 7567–7575.
77 M. F. Foda, L. Huang, F. Shao and H. Y. Han, *ACS Appl. Mater. Interfaces*, 2014, **6**, 2011–2017.
78 R. Marin, A. Vivian, A. Skripka, A. Migliori, V. Morandi, F. Enrichi, F. Vetrone, P. Ceroni, C. Aprile and P. Canton, *ACS Appl. Nano Mater.*, 2019, **2**, 2426–2436.
79 M. J. Roberts, M. D. Bentley and J. M. Harris, *Adv. Drug Delivery Rev.*, 2002, **54**, 459–476.
80 J. V. Jokerst, T. Lobovkina, R. N. Zare and S. S. Gambhir, *Nanomedicine*, 2011, **6**, 715–728.
81 A. J. Keefe and S. Jiang, *Nat. Chem.*, 2012, **4**, 59–63.
82 A. Permadi, Z. Fahmi, J. Chen, J. Chang and C. Cheng, *RSC Adv.*, 2012, **2**, 6018–6022.
83 Y. Kim, Y. Lee, Y. Kim, D. Kim, H. S. Choi, J. C. Park, Y. S. Nam and D. Y. Jeon, *RSC Adv.*, 2017, **7**, 10675–10682.
84 W. Guo, N. Chen, C. Dong, Y. Tu, J. Chang and B. Zhang, *RSC Adv.*, 2013, **3**, 9470–9475.
85 Q. A. Akkerman, A. Genovese, C. George, M. Prato, I. Moreels, A. Casu, S. Marras, A. Curcio, A. Scarpellini, T. Pellegrino, L. Manna and V. Lesnyak, *ACS Nano*, 2015, **9**, 521–531.
86 T. Pons, E. Pic, N. Lequeux, E. Cassette, L. Bezdetnaya, F. Guillemin, F. Marchal and B. Dubertret, *ACS Nano*, 2010, **4**, 2531–2538.
87 J. Yu Lee, D. Heon Nam, M. Hwa Oh, Y. Kim, H. Seok Choi, D. Young Jeon, C. Beum Park and Y. Sung Nam, *Nanotechnology*, 2014, **25**, 175702.
88 Q. Niu, X. Yu, Q. Yuan, W. Hu, D. Yu and Q. Zhang, *Chem. Phys. Lett.*, 2020, **739**, 136977.
89 Y. Feng, L. Liu, S. Hu, Y. Liu, Y. Ren and X. Zhang, *RSC Adv.*, 2016, **6**, 55568–55576.
90 K. D. Wegner and N. Hildebrandt, *Chem. Soc. Rev.*, 2015, **44**, 4792–4834.
91 T. Omata, K. Nose and S. Otsuka-Yao-Matsuo, *J. Appl. Phys.*, 2009, **105**, 073106.
92 H. Zhong, Y. Zhou, M. Ye, Y. He, J. Ye, C. He, C. Yang and Y. Li, *Chem. Mater.*, 2008, **20**, 6434–6443.
93 C. Xia, W. Wu, T. Yu, X. Xie, C. Van Oversteeg, H. C. Gerritsen and C. De Mello Donega, *ACS Nano*, 2018, **12**, 8350–8361.
94 C. M. Hessel, D. Reid, M. G. Panthani, M. R. Rasch, B. W. Goodfellow, J. Wei, H. Fujii, V. Akhavan and B. A. Korgel, *Chem. Mater.*, 2012, **24**, 393–401.
95 J. S. Niezgoda, E. Yap, J. D. Keene, J. R. McBride and S. J. Rosenthal, *Nano Lett.*, 2014, **14**, 3262–3269.
96 J. Niezgoda and M. Harrison, *Chem. Mater.*, 2012, **24**, 3294–3298.
97 I. T. Kraatz, M. Booth, B. J. Whitaker, M. G. D. Nix and K. Critchley, *J. Phys. Chem. C*, 2014, **118**, 24102–24109.
98 D. Deng, Y. Chen, J. Cao, J. Tian, Z. Qian, S. Achilefu and Y. Gu, *Chem. Mater.*, 2012, **24**, 3029–3037.
99 S. O. M. Hinterding, M. J. J. Mangnus, P. T. Prins, H. J. Jöbsis, S. Busatto, D. Vanmaekelbergh, C. De Mello Donega and F. T. Rabouw, *Nano Lett.*, 2021, **21**, 658–665.
100 K. E. Knowles, H. D. Nelson, T. B. Kilburn and D. R. Gamelin, *J. Am. Chem. Soc.*, 2015, **137**, 13138–13147.
101 A. Anand, M. L. Zaffalon, G. Gariano, A. Camellini, M. Gandini, R. Brescia, C. Capitani, F. Bruni, V. Pinchetti, M. Zavelani-Rossi, F. Meinardi, S. A. Crooker and S. Brovelli, *Adv. Funct. Mater.*, 2020, **30**, 1–13.
102 S. B. Zhang, S. H. Wei, A. Zunger and H. Katayama-Yoshida, *Phys. Rev. B: Condens. Matter Mater. Phys.*, 1998, **57**, 9642–9656.
103 J. Park and S. W. Kim, *J. Mater. Chem.*, 2011, **21**, 3745–3750.
104 J. Zhang, R. Xie and W. Yang, *Chem. Mater.*, 2011, **23**, 3357–3361.
105 Z. Liu, A. Tang, M. Wang, C. Yang and F. Teng, *J. Mater. Chem. C*, 2015, **3**, 10114–10120.
106 D. Pan, D. Weng, X. Wang, Q. Xiao, W. Chen, C. Xu, Z. Yang and Y. Lu, *Chem. Commun.*, 2009, 4221–4223.
107 B. Cichy, D. Wawrzynczyk, A. Bednarkiewicz, M. Samoc and W. Strek, *RSC Adv.*, 2014, **4**, 34065–34072.
108 G. B. dos Reis, R. D. F. Rodriguez, C. I. L. dos Santos, L. A. P. Gontijo, M. A. Schiavon, L. De Boni, C. R. Mendonca and M. G. Vivas, *Opt. Mater.*, 2018, **86**, 455–459.
109 K. T. Yong, I. Roy, R. Hu, H. Ding, H. Cai, J. Zhu, X. Zhang, E. J. Bergey and P. N. Prasad, *Integr. Biol.*, 2010, **2**, 121–129.
110 G. Multhaup, A. Schlicksupp, L. Hesse, D. Beher, T. Ruppert, C. L. Masters and K. Beyreuther, *Science*, 1996, **271**, 1406–1409.
111 M. T. Horne and W. A. Dunson, *Arch. Environ. Contam. Toxicol.*, 1995, **29**, 500–505.
112 F. P. Castronovo and H. N. Wagner, *Br. J. Exp. Pathol.*, 1971, **52**, 543–559.
113 F. P. Castronovo and H. N. Wagner, *J. Nucl. Med.*, 1973, **14**, 677–682.
114 H. Li, Z. Chen, J. Li, R. Liu, F. Zhao and R. Liu, *J. Appl. Toxicol.*, 2020, **40**, 1636–1646.
115 M. Nakajima, M. Usami, K. Nakazawa, K. Arishima and M. Yamamoto, *Congenital Anomalies*, 2008, **48**, 145–150.
116 Y. Li, L. Sun, M. Jin, Z. Du, X. Liu, C. Guo, Y. Li and P. Huang, *Toxicol. In Vitro*, 2011, **25**, 1343–1352.
117 D. Napierska, L. C. J. Thomassen, V. Rabolli, D. Lison, L. Gonzalez, M. Kirsch-volders, J. A. Martens and P. H. Hoet, *Small*, 2009, **5**, 846–853.
118 Y. Pan, S. Neuss, A. Leifert, M. Fischler, F. Wen, U. Simon, G. Schmid, W. Brandau and W. Jahnen-dechent, *Small*, 2007, **3**, 1941–1949.
119 S. S. Chetty, S. Praneetha, S. Basu, C. Sachidanandan and A. V. Murugan, *Sci. Rep.*, 2016, **6**, 1–15.
120 B. Zhang, Y. Wang, C. Yang, S. Hu, Y. Gao, Y. Zhang, Y. Wang, H. V. Demir, L. Liu and K. T. Yong, *Phys. Chem. Chem. Phys.*, 2015, **17**, 25133–25141.
121 W. Zou, L. Li, Y. Chen, T. Chen, Z. Yang, J. Wang, D. Liu, G. Lin and X. Wang, *Front. Pharmacol.*, 2019, **10**, 1–10.
122 T. Chen, L. Li, X. Lin, Z. Yang, W. Zou, Y. Chen, J. Xu, D. Liu, X. Wang and G. Lin, *Nanotoxicology*, 2020, **14**, 372–387.

Published on 15 2021. Downloaded on 03.10.2024 13:38:38.

123 Y. Zhang, H. Pan, P. Zhang, N. Gao, Y. Lin, Z. Luo, P. Li, C. Wang, L. Liu, D. Pang, L. Cai and Y. Ma, *Nanoscale*, 2013, **5**, 5919–5929.
124 J. C. Kays, A. M. Saeboe, R. Toufanian, D. E. Kurant and A. M. Dennis, *Nano Lett.*, 2020, **20**, 1980–1991.
125 C. W. Chen, D. Y. Wu, Y. C. Chan, C. C. Lin, P. H. Chung, M. Hsiao and R. S. Liu, *J. Phys. Chem. C*, 2015, **119**, 2852–2860.
126 P. Couvreur and C. Vauthier, *Pharm. Res.*, 2006, **23**, 1417–1450.
127 P. Raghavendra and T. Pullaiah, *Advances in Cell and Molecular Diagnostics*, 2018, pp. 85–111.
128 C. Li and Q. Wang, *ACS Nano*, 2018, **12**, 9654–9659.
129 Q. T. Nguyen, E. S. Olson, T. A. Aguilera, T. Jiang, M. Scadeng, L. G. Ellies and R. Y. Tsien, *Proc. Natl. Acad. Sci. U. S. A.*, 2010, **107**, 4317–4322.
130 M. Y. Berezin and S. Achilefu, *Chem. Rev.*, 2010, **110**, 2641–2684.
131 R. Weissleder, *Nat. Biotechnol.*, 2001, **19**, 316–317.
132 X. Gao, Y. Cui, R. M. Levenson, L. W. K. Chung and S. Nie, *Nat. Biotechnol.*, 2004, **22**, 969–976.
133 C. Zhao, Z. Bai, X. Liu, Y. Zhang, B. Zou and H. Zhong, *ACS Appl. Mater. Interfaces*, 2015, **7**, 17623–17629.
134 K. Yu, P. Ng, J. Ouyang, M. B. Zaman, A. Abulrob, T. N. Baral, D. Fatehi, Z. J. Jakubek, D. Kingston, X. Wu, X. Liu, C. Hebert, D. M. Leek and D. M. Whitfield, *ACS Appl. Mater. Interfaces*, 2013, **5**, 2870–2880.
135 H. S. Choi, Y. Kim, J. C. Park, M. H. Oh, D. Y. Jeon and Y. S. Nam, *RSC Adv.*, 2015, **5**, 43449–43455.
136 M. Howard, B. J. Zern, A. C. Anselmo, V. V. Shuvaev, S. Mitragotri and V. Muzykantov, *ACS Nano*, 2014, **8**, 4100–4132.
137 S. Liu, F. Shi, X. Zhao, L. Chen and X. Su, *Biosens. Bioelectron.*, 2013, **47**, 379–384.
138 S. Liu, S. Pang, W. Na and X. Su, *Biosens. Bioelectron.*, 2014, **55**, 249–254.
139 F. Zhang, P. Ma, X. Deng, Y. Sun, X. Wang and D. Song, *Microchim. Acta*, 2018, **185**, 499.
140 L. Chen, J. Lin, J. Yi, Q. Weng, Y. Zhou, Z. Han, C. Li, J. Chen and Q. Zhang, *Anal. Bioanal. Chem.*, 2019, **411**, 5277–5285.
141 X. Gao, X. Liu, Z. Lin, S. Liu and X. Su, *Analyst*, 2012, **137**, 5620–5624.
142 Z. Lin, Z. Liu, H. Zhang and X. Su, *Analyst*, 2015, **140**, 1629–1636.
143 D. V. Makarov, S. Loeb, R. H. Getzenberg and A. W. Partin, *Annu. Rev. Med.*, 2009, **60**, 139–151.
144 H. Zhang, Y. Wu, Z. Gan, Y. Yang, Y. Liu, P. Tang and D. Wu, *J. Mater. Chem. B*, 2019, **7**, 2835–2844.
145 S. Plunkett, M. El Khatib, İ. Şencan, J. E. Porter, A. T. N. Kumar, J. E. Collins, S. Sakadžić and S. A. Vinogradov, *Nanoscale*, 2020, **12**, 2657–2672.
146 J. V. Frangioni, S. W. Kim, S. Ohnishi, S. Kim and M. G. Bawendi, *Methods Mol. Biol.*, 2007, **374**, 147–159.
147 S. Kim, Y. T. Lim, E. G. Soltesz, A. M. De Grand, J. Lee, A. Nakayama, J. A. Parker, T. Mihaljevic, R. G. Laurence, D. M. Dor, L. H. Cohn, M. G. Bawendi and J. V. Frangioni, *Nat. Biotechnol.*, 2004, **22**, 93–97.
148 H. Fujii, Y. Kitagawa, M. Kitajima and A. Kubo, *Ann. Nucl. Med.*, 2004, **18**, 1–12.
149 L. Josephson, U. Mahmood, P. Wunderbaldinger, Y. Tang and R. Weissleder, *Mol. Imaging*, 2004, **2**, 18–23.
150 M. G. Panthani, T. A. Khan, D. K. Reid, D. J. Hellebusch, M. R. Rasch, J. A. Maynard and B. A. Korgel, *Nano Lett.*, 2013, **13**, 4294–4298.
151 R. N. Palumbo and C. Wang, *Curr. Drug Delivery*, 2006, **3**, 47–53.
152 S. Bouccara, A. Fragola, E. Giovanelli, G. Sitbon, N. Lequeux, T. Pons and V. Loriette, *J. Biomed. Opt.*, 2014, **19**, 051208.
153 R. Yusuf, D. Co, W. Zaher, L. J. Mortensen, C. Alt, S. A. Vinogradov, D. T. Scadden and C. P. Lin, *Nature*, 2014, **508**, 269–273.
154 G. Mandal, M. Darragh, Y. A. Wang and C. D. Heyes, *Chem. Commun.*, 2013, **49**, 624–626.
155 L. Prodi, E. Rampazzo, F. Rastrelli, A. Speghini and N. Zaccheroni, *Chem. Soc. Rev.*, 2015, **44**, 4922–4952.
156 M. Montalti, L. Prodi, E. Rampazzo and N. Zaccheroni, *Chem. Soc. Rev.*, 2014, **43**, 4243–4268.
157 M. Wang, Z. Chen and C. Cao, *Mater. Lett.*, 2014, **120**, 50–53.
158 J. C. Hsu, C. C. Huang, K. L. Ou, N. Lu, F. Der Mai, J. K. Chen and J. Y. Chang, *J. Mater. Chem.*, 2011, **21**, 19257–19266.
159 G. Manna, S. Jana, R. Bose and N. Pradhan, *J. Phys. Chem. Lett.*, 2012, **3**, 2528–2534.
160 Q. Liu, R. Deng, X. Ji and D. Pan, *Nanotechnology*, 2012, **23**, 255706.
161 Y. Zheng, Y. Zou and J. Jiang, *Mater. Lett.*, 2016, **168**, 86–89.
162 Y. Yang, L. Lin, L. Jing, X. Yue and Z. Dai, *ACS Appl. Mater. Interfaces*, 2017, **9**, 23450–23457.
163 C. Y. Cheng, K. L. Ou, W. T. Huang, J. K. Chen, J. Y. Chang and C. H. Yang, *ACS Appl. Mater. Interfaces*, 2013, **5**, 4389–4400.
164 W. Yang, W. Guo, X. Gong, B. Zhang, S. Wang, N. Chen, W. Yang, Y. Tu, X. Fang and J. Chang, *ACS Appl. Mater. Interfaces*, 2015, **7**, 18759–18768.
165 K. Tanha, A. M. Pashazadeh and B. W. Pogue, *Biomed. Opt. Express*, 2015, **6**, 3053.
166 J. Axelsson, S. C. Davis, D. J. Gladstone and B. W. Pogue, *Med. Phys.*, 2011, **38**, 4127–4132.
167 Y. Xu, H. Liu and Z. Cheng, *J. Nucl. Med.*, 2011, **52**, 2009–2018.
168 Y. Bernhard, B. Collin and R. A. Decréau, *Chem. Commun.*, 2014, **50**, 6711–6713.
169 Z. Ranjbar-Navazi, Y. Omidi, M. Eskandani and S. Davaran, *TrAC, Trends Anal. Chem.*, 2019, **118**, 386–400.
170 S. M. Janib, A. S. Moses and J. A. MacKay, *Adv. Drug Delivery Rev.*, 2010, **62**, 1052–1063.
171 X. Gao, Z. Liu, Z. Lin and X. Su, *Analyst*, 2014, **139**, 831–836.
172 A. A. P. Mansur, J. C. Amaral-Júnior, S. M. Carvalho, I. C. Carvalho and H. S. Mansur, *Carbohydr. Polym.*, 2020, **247**, 116703.

 This journal is © The Royal Society of Chemistry 2021

173 G. Lv, W. Guo, W. Zhang, T. Zhang, S. Li, S. Chen, A. S. Eltahan, D. Wang, Y. Wang, J. Zhang, P. C. Wang, J. Chang and X. J. Liang, *ACS Nano*, 2016, **10**, 9637–9645.
174 V. Ntziachristos and D. Razansky, *Chem. Rev.*, 2010, **110**, 2783–2794.
175 Z. Liu, N. Chen, C. Dong, W. Li, W. Guo, H. Wang, S. Wang, J. Tan, Y. Tu and J. Chang, *ACS Appl. Mater. Interfaces*, 2015, **7**, 18997–19005.
176 Z. Lin, Q. Ma, X. Fei, H. Zhang and X. Su, *Anal. Chim. Acta*, 2014, **818**, 54–60.

Published on 15 2021. Downloaded on 03.10.2024 13:38:38.